Marginal zone B cells control the response of follicular helper T cells to a high cholesterol diet

Meritxell Nus[1], Andrew P. Sage[1], Yuning Lu[1], Leanne Masters [1], Brian Y. H. Lam[2], Stephen Newland[1], Sandra Weller[3], Dimitrios Tsiantoulas[4,5], Juliette Raffort[1], Damiënne, Marcus[1], Alison Finigan[1], Lauren Kitt[1], Nichola Figg[1], Reinhold Schirmbeck[6], Manfred Kneilling[7,8], Giles S. H. Yeo[2], Christoph J. Binder[4,5], José Luis de la Pompa[9,10], Ziad Mallat[1,11]

[1]Division of Cardiovascular Medicine, University of Cambridge, UK.

[2]Metabolic Research Laboratories, University of Cambridge and MRC Metabolic Diseases Unit, Wellcome-MRC Institute of Metabolic Science, UK

[3]Institut Necker-Enfants Malades, INSERM U1151-CNRS UMR 8253, Sorbonne Paris Cité, Université Paris Descartes, Paris, France

[4]Department of Laboratory Medicine, Medical University of Vienna, Austria

[5]Center for Molecular Medicine (CeMM) of the Austrian Academy of Sciences, Austria

[6]Department of Internal Medicine I, Ulm University Hospital, Ulm, Germany

[7]Department of Preclinical Imaging and Radiopharmacy, Werner Siemens Imaging Center, Eberhard Karls University, Tübingen, Germany

[8]Department of Dermatology, Eberhard Karls University, Tübingen, Germany

[9]Intercellular Signalling in Cardiovascular Development & Disease Lab, Centro Nacional de Investigaciones Cardiovasculares Carlos III (CNIC), Madrid, Spain

[10]Centro de Investigación Biomédica en Red de Enfermedades Cardiovasculares, Spain

[11]Institut National de la Santé et de la Recherche Médicale (Inserm), Unit 970, Paris Cardiovascular Research Center, Paris, France.

Correspondence should be addressed to: Ziad Mallat, MD, PhD, at Division of Cardiovascular Medicine, University of Cambridge, Addenbrooke's Hospital, Cambridge, CB2 2QQ, UK. E-Mail: zm255@medchl.cam.ac.uk.

ABSTRACT

Splenic marginal zone B (MZB) cells, positioned at the interface between the circulating blood and lymphoid tissue, detect and respond to blood-borne antigens. Here, we show that MZB cells in mice activate a homeostatic program in response to a high cholesterol diet (HCD), and regulate both T follicular helper (Tfh) cell differentiation and accumulation. HCD feeding upregulated MZB cell surface expression of the immunoregulatory ligand PDL1 in an ATF3-dependent manner and increased the interaction between MZB cells and (pre-)Tfh cells, leading to PDL1-mediated suppression of Tfh cell motility, alteration of Tfh cell differentiation, reduced Tfh abundance and suppression of the pro-atherogenic Tfh response. Our findings reveal a previously unsuspected role for MZB cells in controlling the Tfh–germinal center response to a cholesterol-rich diet, and uncover a PDL1-dependent mechanism by which MZB cells use their innate immune properties to limit an exaggerated adaptive immune response.

The development of atherosclerotic arterial lesions in response to elevated circulating lipid levels is characterized by an inflammatory activation of the vascular wall, and is associated with the induction of innate and adaptive immune responses directed at least in part towards (modified) lipoproteins [1,2]. More specifically, B lymphocyte-dependent immune responses play prominent roles in atherosclerosis. B1-derived natural IgM antibodies have consistently been shown to be athero-protective (reviewed in [3,4]). In contrast, B2 cell responses promote atherogenesis [5-8] through their support of pro-atherogenic T cells [5]. So-called regulatory B cells originate from the B2 cell compartment and are involved in the control of exaggerated adaptive immune responses [9-11]. However, their developmental pathway is not well understood and their contribution to atherosclerosis is still uncertain [12,13]. Importantly, there are 2 major B2 cell subsets, follicular (FOB) and the marginal zone B (MZB) cells, with distinct developmental pathways and functional properties [14]. While the contribution of adaptive FOB cells to the development of atherosclerosis can be inferred from their roles in the support of pro-atherogenic T follicular helper (Tfh) cells and germinal center (GC) responses [15], the potential contribution of innate-like MZB cells to the regulation of the immune response to high cholesterol diet (HCD) cannot be easily predicted and remains almost unexplored, apart from the reported ability of this B2 cell subset to mount T-independent responses to (modified) lipoproteins (e.g., oxidized phosphatidylcholine epitopes) [16].

RESULTS

MZB cells limit the development of atherosclerosis through inhibition of the Tfh response

To address the role of MZB cells in atherosclerosis, we generated mice with B cell lineage-specific (*Cd79a*$^{Cre/+}$) conditional deletion of the gene *Rbpjk* (*Rbpjk*$^{flox/flox}$), which encodes the effector transcription factor downstream of the Notch2 receptor and which is known to be required for MZB cell development [17-19]. We then reconstituted lethally-irradiated low-density lipoprotein receptor deficient (*Ldlr*$^{-/-}$) mice with bone marrow from either *Cd79a*$^{Cre/+}$*;Rbpjk*$^{flox/flox}$ or *Cd79a*$^{+/+}$*;Rbpjk*$^{flox/flox}$ control mice. After recovery, these mice were put on a HCD for 8 weeks or 16 weeks. In *Cd79a*$^{Cre/+}$*;Rbpjk*$^{flox/flox}$ mice, disruption of Notch signaling in B cells induced a selective depletion of splenic MZB cells (Fig. 1a and Supplementary Fig. 1a) and markedly accelerated the development of both early (Fig. 1b and Supplementary Fig. 1b) and advanced atherosclerotic lesions (Fig. 1c) as compared to control mice, despite not having effects on plasma lipid parameters (Supplementary Fig. 1c-f). Analysis of plaque composition showed sustained accumulation of macrophages and CD3$^+$ T cells in the lesions of MZB cell-deficient mice (Supplementary Fig. 1g-j). We detected only subtle changes in antibody responses against modified LDL (Supplementary Fig. 1k-n), which could not account for the marked acceleration of atherosclerosis in MZB cell-deficient animals. The abundance of neutrophils (Supplementary Fig. 2a) and monocytes/macrophages (Supplementary Fig. 2b, c) in the spleen were similar between MZB-cell deficient and control mice. We therefore assessed the effect of MZB cell deficiency on peripheral T cell activation status, and found that MZB cell-deficient mice had increased percentages of splenic CD4$^+$ T effector memory CD44^{hi}CD62L$^-$ cells (Fig. 2a) and Th2 cells (Supplementary Fig. 2d)

with a trend towards an increased percentage of Th1 but no change in the percentages of Th17 and regulatory T cells (Supplementary Fig. 2e-g), as compared to control mice. Intriguingly, we also found a substantial accumulation of Tfh cells ($CD4^{+}CXCR5^{hi}PD1^{hi}$) in the spleens of MZB deficient mice (Fig. 2b), whereas the percentage of Tfh cells was not significantly higher in lymph nodes of MZB as compared to control mice (1.78±0.4% of $CD4^{+}$ T cells, n=7, versus 0.93±0.18%, n=8, respectively; p=0.061). Moreover, irradiated *Ldlr*$^{-/-}$ mice that had been maintained on a chow diet for 8 weeks did not display an increased percentage of splenic Tfh cells (0.54±0.057%) in comparison to *Ldlr*$^{-/-}$ mice fed a HCD, indicating that HCD is required for induction of a Tfh response. Notably, MZB cell-deficiency did not accelerate the development of atherosclerosis in the absence of $CD4^{+}$ T cells (Fig. 2c). Furthermore, selective Tfh cell depletion using an anti-ICOSL neutralizing antibody (Supplementary Fig. 2h-k) abrogated the acceleration of atherosclerosis in MZB cell-deficient mice (Fig. 2d), highlighting the role of the Tfh cell response in the pro-atherogenic phenotype caused by MZB cell deficiency. *Ldlr*$^{-/-}$ mice reconstituted with *Cd79a*$^{Cre/+}$ bone marrow did not show an increase in Tfh cell numbers or atherosclerotic lesion size after 8 weeks on a HCD, as compared to mice reconstituted with *Cd79a*$^{+/+}$ bone marrow (data not shown), indicating that deletion of one *Cd79a* allele does not alter the Tfh response or the development of atherosclerosis.

A high cholesterol diet activates a homeostatic and anti-inflammatory program in MZB cells

As modulation of Tfh responses by MZB cells has not been described previously, we used an unbiased approach to gain mechanistic insight. After sorting MZB cells from

Ldlr$^{-/-}$ mice after 8 weeks on chow diet or HCD and performing RNA sequencing (RNA-seq), we found that 71 genes were significantly upregulated and 21 genes were significantly downregulated ($p < 0.0004$; $q < 0.01$ for all up- and down-regulated genes) in MZB cells after HCD (Fig. 3a-b). Among the highly regulated genes were genes involved in B cell receptor (BCR) signaling, B cell activation, cell cycle regulation and trafficking (e.g., *Nr4a1*, *Egr1*, *Fos*, *Junb*, *Klf2*, *Klf4*, *Rap1b*, *Cd69*), communication between the innate and adaptive immune systems (e.g., *Ccr7*, *Cd83*, *Cd274*), lipid metabolism (e.g., *Abcg1*, *Atf3*, *Nr4a1*) and regulation of immune and inflammatory responses (e.g., *Fos/Fosb*, *Jun/Junb*, *Crem*, *Atf3*, *Tnfaip3*, *Nfkbid*, *Dusp1*, *Dusp4*, *Il10*). Intriguingly, we also found a significant induction of pathways that are critical for the maintenance of metabolic and immune homeostasis, notably the NF-κB (*Tnfaip3*, *Nfkibd*, *Atf3*, *Nr4a1*, *Dusp1/4*) and AP1 (*Fos*, *Jun*, *Atf3*, *Crem*, *Dusp1/4*) pathways.

ATF3 expression in MZB cells control Tfh cell accumulation in response to HCD and is required for the atheroprotective effect of MZB cells

The gene encoding ATF3, a member of the CREB/ATF family of transcription factors, was the most highly upregulated transcription factor gene in MZB cells after HCD (Fig. 3a) and bioinformatic analysis indicated that ATF3 could potentially link several pathways downstream of innate and adaptive immune receptors (Fig. 3c-d). ATF3 regulation of metabolic and immune pathways is well documented in cell types other than B cells, most notably in macrophages. In response to lipid loading, ATF3 suppresses the transcription of *Ch25h*, which encodes the enzyme cholesterol 25-hydroxylase that converts cholesterol into 25-hydroxycholesterol, thereby limiting foam cell formation [20];

in response to stimulation with HDL-cholesterol or downstream of TLR4 activation (which can be triggered by macrophage treatment with oxLDL or free fatty acids), ATF3 interacts with NF-κB1 and AP1 to induce a major negative feedback loop and shut down pro-inflammatory responses[21,22]. These regulatory functions of ATF3 are consistent with our finding that *Atf3* upregulation in MZB cells after HCD was accompanied by negative regulation of TLR signaling (analysis with Ingenuity software, $p=1.38x10^{-3}$) (Fig 3c). Moreover, we found that the NF-E2 related factor 2 (NRF2)-mediated oxidative stress response was the most significantly activated Ingenuity canonical pathway in MZB cells after HCD ($p=3.02x10^{-4}$) (Fig 3c), consistent with a previous report that *Atf3* is strongly induced by NRF2 in response to reactive oxygen species (ref. 23). Thus, our data suggest a potentially dominant role for ATF3 in orchestrating the regulatory program induced in MZB cells after HCD.

The function of ATF3 in B lymphocytes is unknown. Since HCD increases the level of circulating endotoxin in mice (Supplementary Fig. 3a) and humans (reviewed in [24]), we analyzed the response of WT and *Atf3*$^{-/-}$ MZB cells to LPS. *Il6* is a prototypical TLR4-induced inflammatory gene that is directly repressed by ATF3 in macrophages [21,22]. We found that ATF3 similarly limits *Il6* expression in LPS-treated MZB cells (Fig. 4a). We also found that ATF3 deficiency in MZB cells prevented LPS-induced upregulation of both gene and protein expression of PDL1 (encoded by *Cd274*) (Fig. 4b, c), a ligand for PD1 (encoded by *Pdcd1*) and a potential regulator of the Tfh response [25].

To examine the impact of ATF3 deficiency in MZB cells on the immune response to HCD *in vivo*, we reconstituted lethally-irradiated *Ldlr*$^{-/-}$ mice with bone marrow from *Cd79a*$^{Cre/+}$*;Rbpjk*$^{flox/flox}$ mice (the 'no MZB' group) and compared them to *Ldlr*$^{-/-}$ mice reconstituted with mixed bone marrow containing 80% *Cd79a*$^{Cre/+}$*;Rbpjk*$^{flox/flox}$ bone marrow + either 20% wild-type bone marrow (the 'WT MZB' group) or 20% *Atf3*$^{-/-}$ bone marrow (the '*Atf3*$^{-/-}$ MZB' group) (see Methods). As expected, MZB cells were completely absent in the no MZB group and were fully reconstituted in the WT MZB and *Atf3*$^{-/-}$ MZB groups (Supplementary Fig. 3b). Consistent with the *in vitro* data, PDL1 expression was markedly reduced on reconstituted *Atf3*$^{-/-}$ MZB cells compared to WT MZB cells (Fig. 4d-e). Reconstitution of MZB-deficient mice with WT MZB cells significantly reduced the accumulation of Tfh and GC B cells in the spleen (Fig. 4f-g) and fully rescued the accelerated atherosclerosis phenotype caused by MZB cell deficiency (Fig. 4h-i), despite not having effects on plasma cholesterol levels (Supplementary Fig. 3c) or plaque composition (Supplementary Fig. 3d-e). However, reconstitution with *Atf3*-deficient MZB cells was unable to limit the pro-atherogenic Tfh/GC response of MZB cell deficiency (Fig. 4f-i), providing direct evidence for the critical regulatory and homeostatic roles of ATF3 expression in MZB cells in response to HCD.

MZB cells limit Tfh cell motility through upregulation of PDL1

We next examined whether a direct interaction between MZB and T cells is required to limit the Tfh response. We hypothesized that MZB cells may need to migrate to the splenic follicle in order to interfere with Tfh cells. MZB cells continuously shuttle

between the marginal zone and the follicle, and CXCR5 expression on MZB cells is required to induce their translocation into the follicle upon downregulation of S1PR1 [26]. We therefore reconstituted *Ldlr*$^{-/-}$ MZB-deficient mice with *Cxcr5*$^{-/-}$ or WT MZB cells (see Methods). MZB cell reconstitution was similar between *Cxcr5*$^{-/-}$ and WT MZB groups (7.42±1.68% and 6.81±0.64%, respectively, n=8 in each group). In contrast to our expectation, *Cxcr5* deletion in MZB cells did not impair their ability to reduce Tfh cell accumulation (3.52% and 3.54% in the WT and *Cxcr5*$^{-/-}$ MZB cells groups, respectively n=8 in each group), suggesting that MZB cell shuttling to the follicle is not required for the inhibitory role of MZB cells on Tfh cell accumulation.

We therefore hypothesized that MZB cells may exert their control on the Tfh response by interacting with (pre)-Tfh cells in the T cell zone or at the T-B border of the spleen, prior to Tfh translocation into the follicle. B cell movement into the T cell zone and to the T-B border requires the coordinated actions of the CCR7 and EBI2 receptors (reviewed in [27,28]). Cell-sorted MZB cells, but not FOB cells, recovered from *Ldlr*$^{-/-}$ mice showed increased expression of *Ccr7* and *Ebi2* in response to HCD as compared to chow diet (Supplementary Fig. 4a-b), suggesting that HCD might promote MZB cell movement into the T cell zone and the T-B border [27,28]. Consistent with this hypothesis, we found that HCD led to increased accumulation of IgM^{hi} MZB-like cells at the boundary of the T cell zone, where IgM^{hi} B cells established close cell-cell contacts with CXCR5^{+}CD4^{+} T cells (Supplementary Fig. 4c-d).

We next sought to test whether physical interaction of MZB and Tfh cells is required for downregulation of the Tfh response. In studying the interaction between MZB and Tfh cells, we focused on the PDL1/PD1 axis for several reasons. MZB cells express the highest level of PDL1 of the B cell subsets tested (Supplementary Fig. 5a), and we noted in the RNA-seq data that HCD led to upregulation of *Cd274* expression in MZB cells, a finding that was confirmed by qPCR and cell surface expression data (Fig. 5a). Notably, in FOB cells, HCD led to upregulation of *Icosl* but not *Cd274* (Fig. 5b), which is of interest in the context of previous findings showing that ICOS and PD1 signaling have contrasting roles in Tfh cells; the former is required for instructing Tfh cell differentiation (reviewed in [29]), whereas the latter limits the number of Tfh cells and regulates the survival of GC B cells [25].

When we cultured sorted and labeled Tfh cells *in vitro* with cell-sorted MZB or FOB cells (all from immunized wild type mice, see Methods), we found that co-culture with MZB cells resulted in significantly lower levels of Tfh cell velocity and motility, as compared to co-culture with FOB cells (Fig. 5c-d). Moreover, contact time and the number of Tfh cells interacting with B cells were significantly higher when Tfh cells were co-cultured with MZB as compared to FOB cells (Fig. 5e). These differences were abrogated when a blocking anti-PDL1 antibody was added to the co-culture (Fig. 5c-e), indicating that the inhibitory effect of MZB on Tfh relies on PDL1. Our results are consistent with previous work that reported PD1-dependent immune exhaustion through induction of antiviral T cell motility paralysis [30]. In another experiment, we found that incubation of Tfh cells with MZB cells from *Ldlr*$^{-/-}$ mice fed HCD significantly decreased

Tfh cell velocity and increased contact time, in comparison to incubation with MZB cells from *Ldlr*$^{-/-}$ mice fed chow diet (Supplementary Fig. 5b, c), consistent with the upregulation of PDL1 expression in MZB cells after HCD.

BCR signaling promotes PDL1 expression in MZB cells

We were interested by the high expression of PDL1 on MZB as compared to FOB cells. Those B cell subsets may differ in BCR signaling strength, and the BCR signaling pathway was modulated in MZB cells after HCD. Indeed, we found that direct engagement of IgM on purified MZB cells increased both gene and protein expression of PDL1, and these effects were dependent on Btk activation (Supplementary Fig. 6a-d). We next examined human circulating MZB-like cells [31,32] and found that they expressed higher levels of PDL1 as compared to circulating naïve B cells (Supplementary Fig. 6e). Stimulation of BCR signaling further induced PDL1 expression in these human MZB-like cells (Supplementary Fig. 6f, g). We also noted that human splenic MZB cells [31,32] expressed much higher levels of PDL1 as compared to naïve splenic B cells (Supplementary Fig. 6h). We conclude both murine and human MZB cells show comparatively high levels of PDL1 expression compared to other B cell populations, and that PDL1 expression in MZB cells is regulated by BCR signaling

MZB cells control the pro-atherogenic Tfh-GC response through upregulation of PDL1

To address the direct role of MZB cell-restricted PDL1 expression in modulation of the Tfh-GC response *in vivo*, we reconstituted MZB-deficient *Ldlr*$^{-/-}$ mice with WT or

Cd274$^{-/-}$ MZB cells (see Methods). Similar levels of MZB cell reconstitution was achieved in the 2 groups of mice (Supplementary Fig. 7a). As expected, PDL1 expression was almost abrogated on reconstituted MZB cells in the *Cd274*$^{-/-}$ MZB group as compared to the WT MZB group (Supplementary Fig. 7b). Strikingly, reconstitution of *Ldlr*$^{-/-}$ with *Cd274*-deficient MZB cells was unable to limit the Tfh-GC response to HCD (Fig. 5f-g), such that the *Cd274*$^{-/-}$ MZB group had more severe atherosclerosis as compared to the WT group **[**(Fig. 5h and Supplementary Fig. 7c-g), providing evidence that PDL1 expression in MZB cells limits the pro-atherogenic Tfh response.

MZB cell deficiency alters the Tfh cell program

We were surprised by the absence of a clear increase in antibody levels (Supplementary Fig. 1k-n) despite the increased numbers of Tfh cells in MZB-deficient mice after HCD. This finding is reminiscent of the effects of PD1 deficiency in T cells [25], which led to an increase in Tfh cell numbers but an impairment of Tfh quality; in particular, PD1-deficient Tfh cells had reduced production of IL-21, a cytokine that is required for optimal antibody responses [33]. This previous work fits with our identification of a major role of MZB-restricted PDL1 expression in the regulation of the Tfh response, through interaction of PDL1 on MZB cells with PD1 on Tfh cells.

To better characterize the Tfh cells that develop in MZB-deficient mice after HCD, we performed RNA-seq on cell-sorted spleen Tfh cells after 8 weeks on HCD in lethally-irradiated *Ldlr*$^{-/-}$ mice reconstituted with bone marrow from *Cd79a*$^{Cre/+}$*;Rbpjk*$^{flox/flox}$ mice (the 'no MZB' group) or from *Cd79a*$^{+/+}$*;Rbpjk*$^{flox/flox}$ mice (the 'WT MZB' group). We

focused on the expression of a subset of genes associated with, or directly involved in the determination of Tfh cell identity. We did not find significant differences in the expression of *Bcl6*, *Cxcr5* and *Pdcd1* between the two groups, although we found a tendency towards reduced *Bcl6* (p=0.07) and *Cxcr5* (p=0.14) expression in the no MZB group compared to the WT MZB group. Notably, we found a significant reduction of *Il21* expression in the no MZB group (Fig. 6a, b), supporting the hypothesis that the quality of Tfh cells from MZB-deficient mice is impaired, and providing a plausible explanation for the absence of an overt increase in antibody response, despite increased Tfh cell numbers, in MZB-deficient animals. Further analysis of the RNA-seq data revealed differences in the expression of major transcription factors and pathways involved in the control of Tfh cell differentiation between the two groups of mice (Fig. 6): genes that limit the differentiation of Tfh cells were upregulated in the no MZB group, whereas pathways that promote Tfh cell development were downregulated. For example, recent studies have identified an important role for KLF2 in limiting the differentiation of Tfh cells through induction of *S1pr1* [34], and expression of both *Klf2* and *S1pr1* were significantly upregulated (at least 2-fold) in the no MZB group (Fig. 6a,b). In contrast to *S1pr1*, we found that expression of *S1pr2*, which supports Tfh cell differentiation and promotes Tfh cell retention in GCs [35], was substantially reduced in the no MZB group (Fig. 6a, d). Decreased expression of S1PR2 in Tfh cells is associated with decreased expression of *Il21* but higher expression of *Ccr7*, *Ccr6*, *S1pr1* and *Sell* [35], a pattern that we also observed in the no MZB group (Fig. 6a). Furthermore, expression of *Icos*, which downregulates *Klf2* [36], and *Maf*, which promotes the expression of several Tfh cell-related genes, including *Il21* and *Cxcr5* [37], were both significantly downregulated in the

no MZB group (Fig. 6a, b, d). Finally, expression of *Ascl2*, which interacts with BATF/IRF4 to orchestrate the Tfh program through induction of CXCR5 and suppression of CCR7 expression and IL-2 signaling [38], was significantly downregulated in the no MZB group, along with downregulated expression of *Irf4* and upregulated expression of *Ccr7* and *Il2ra* (Fig. 6). Differential regulation of *Icos* and *Il2ra* may control the bifurcation between effector Th and Tfh programs [39], a concept which is in agreement with the over-representation of those pathways in the Ingenuity canonical pathway analysis of the RNA-seq data (Fig. 6c).

DISCUSSION

Only a few previous studies have addressed the role of MZB cells in a hypercholesterolemic context [16,40]. MZB cell abundance increases in the spleens of hypercholesterolemic *Apoe*$^{-/-}$ mice compared to wild type animals, due in part to decreased IFNγ release by iNKT cells [40]. MZB cells also ingest modified LDL and mount extra-follicular antibody responses against oxidation-specific epitopes [16]. However, the contribution of MZB cells to atherosclerosis was unexplored. Our results identify a critical role for MZB cells in the establishment of an optimal Tfh program in response to HCD, limiting exaggerated adaptive immune responses and substantially halting the development and progression of atherosclerosis.

These findings raise several important questions that require further exploration. For example, what signals activate MZB cells after HCD? Our RNA-seq data point to the involvement of the TLR and BCR signaling pathways. One potential factor leading to

MZB cell activation after HCD is diet-induced translocation of endotoxin from the gut to the circulation, but there are many other possibilities, including activation by oxidation-specific epitopes from modified self proteins and lipids, and the direct or indirect impact of the gut microbiota. In this regard, a recent study reported induction of regulatory B cells by gut microbiota-driven IL-1β and IL-6 [41]. Thus, a better understanding of the major determinants of MZB cell activation after HCD is needed.

In view of our findings that, in HCD-fed mice, MZB cells leave the marginal zone and interact with (pre)Tfh cells, it will be important to study the signals that instruct the MZB cells to leave the marginal zone and guide them to Tfh cells. In this regard, we did not observe downregulation of *S1pr1* expression or increased expression of *Cxcr5*, the major receptors that control the shuttling of MZB cells between the marginal zone and the follicle [26]. Moreover, *Cxcr5* deletion in MZB cells did not alter their ability to regulate the Tfh cell response. Our data point to other possible mechanisms: for example, as expression of *Cd69*, which suppresses the function of S1PR1 [42], was highly upregulated in MZB cells after HCD, it may be responsible for MZB cell egress from the marginal zone. On the other hand, MZB cells after HCD also upregulate CCR7 and EBI2, the latter of which is a receptor for oxysterols [43,44]; CCR7 and EBI2 may facilitate MZB cell movement to the T cell zone and the T-B border, respectively.

Our findings indicate that PDL1 expression in MZB cells regulates Tfh cell motility through induction of PD1 signaling in (pre)-Tfh cells. Previous work has unraveled a critical role for ICOSL expression on FOB cells in ICOS-driven T cell motility at the T-B

border, whereby FOB cells promote the recruitment of Tfh cells into the follicle [45]. In this regard, the differential upregulation of *Cd274* and *Icosl* in MZB compared with FOB cells (Fig. 5a-b) suggests that FOB and MZB cells have contrasting roles in response to HCD: FOB cells promote Tfh cell development whereas MZB cells shut down any exaggerated activation of the Tfh response.

Our results agree with previous studies that reported increased pro-atherogenic T cell responses in mice after combined deficiency of PDL1 and PDL2 [46] or after impairment of PD1 [47]. However, the mechanisms proposed in these previous studies differed and were attributed mainly to macrophage or dendritic cell-dependent alteration of T cell activation. Our results substantially extend these previous findings by identifying PDL1 expression in MZB cells as a major regulator of the pro-atherogenic Tfh response. Our results are also in agreement with a recent study that reported regulation of Tfh cells by B cells expressing high levels of PDL1 in a setting of experimental autoimmune encephalomyelitis [48]. However, the specific role of MZB cells in the regulation of immune responses in this context was not reported.

Our work identifies an important role for MZB cells in the regulation of the Tfh cell program, but additional work will be required to fully address the mechanisms through which MZB cells control Tfh differentiation. For example, expression of the transcription factor BLIMP1 was downregulated in Tfh cells of MZB deficient mice. As this transcription factor is an antagonist of BCL6 and a major inhibitor of Tfh differentiation [49], it will be interesting to study the mechanisms underlying its downregulation. Although

PD1 signaling in Tfh cells has been reported to regulate follicular regulatory T cells in blood and lymph nodes [50], we did not find an effect of MZB deficiency on *Foxp3* expression in Tfh cells (data not shown), suggesting little or no effect of MZB deficiency on regulatory Tfh cells. However, we did detect reduced expression of *Ctla4* in Tfh cells of MZB deficient animals (Figure 6a), suggesting increased susceptibility of Tfh cells to activation, consistent with the increased number of effector memory T cells in the absence of MZB cells (Figure 2a).

Our work did not address the mechanisms through which Tfh cells promote atherogenesis when released from the negative regulatory influence of MZB cells. The changes caused by MZB cell deficiency in the levels of circulating antibodies directed against oxidation epitopes were variable, and did not correlate with the acceleration of atherosclerosis. However, a more detailed assessment of the humoral response in MZB cell-deficient mice should be carried out before reaching any definite conclusions about the contribution of the GC response to the atherosclerotic phenotype of these mice.

In conclusion, this work reveals a new role for MZB cells in maintaining immune homeostasis in response to a HCD through activation of a regulatory program affecting both the quantity and quality of Tfh cells. MZB cells appear to be required for optimal Tfh cell differentiation while restraining the Tfh response. Absence of MZB cells leads to excessive accumulation of sub-optimally differentiated Tfh cells and increased levels of Th and T effector memory cells. These results may have important implications to our

understanding of the impact of environmental influences, such as variations in diet composition, on the initiation and/or progression of immune-mediated diseases.

METHODS

Please see a full description of Materials and Methods in the online version of the paper in Supplementary data.

Accesion Codes

MZB cells and Tfh cells RNAseq data at GSE71699.

Data Availability Statement

The data of the findings of this study are available from the corresponding author upon reasonable request.

ACKNOWLEDGEMENTS

This work was supported by BHF grant no. PG/15/76/31756, ERC grant no. 2891164 and EC FP7 VIA grant no. HEALTH-F4-2013-603131 to Z.M. and SAF2013-45543-R from the Spanish Ministry of Economy and Competitiveness (MINECO) to J.L.dlP. M.N. was first supported by a Sara Borrell grant (CD09/00452) from Instituto Nacional de Salud Carlos III (Spain) and then by a 2-year BHF Project Grant. M.N. has also received funding from the People Programme (Marie Curie Actions) of the European Union's Seventh Framework Programme (FP7/2007-2013) under REA grant agreement n° 608765. We acknowledge measurements of lipids in blood to Keith Burling. The Wellcome Trust supported Cambridge Mouse Biochemistry Laboratory. We acknowledge Prof. Anna Petrunkina, Esther Perez, Christopher Bowman, Simon McCallum, Jelena Markovic Djuric and Natalia Savinykh in the Phenotyping Hub of the

Dept. of Medicine (University of Cambridge) for their help in flow cytometry and sorting, and Maria Ozsvar Kozma (Department of Laboratory Medicine, Medical University of Vienna, Austria) for help in antibody measurements. We also acknowledge Marcella Ma for support during libraries preparation for RNAseq.

Author contributions: M.N. and Z.M. conceived the study; M.N. designed, performed and analysed experiments; A.S. performed experiments and provided advise on design and discussion; Y.L. performed time lapse microscopy experiments; S.N., J.R. and D.M. performed experiments; L.M., A.F., L.K. and N.F. helped with flow cytometry, animal work and histochemistry respectively; S.W. provided and analysed human spleens crucial to this study; D.T. performed blood antibody measurements; R.S., M.K. and JLP, provide mice and cells crucial for the paper; B.Y.H.L. performed bioinformatics RNAseq analysis; G.S.H.Y supervised RNAseq analysis; C.B. helped with the discussion of the paper and give advise on antibodies measurement; Z.M. supervised all the study; M.N. and Z.M. prepared the manuscript; all authors contributed to and approved the final manuscript.

Competing financial interest statement: The authors have no conflicting financial interests to disclose.

REFERENCES

1. Libby, P., Lichtman, A.H. & Hansson, G.K. Immune effector mechanisms implicated in atherosclerosis: from mice to humans. *Immunity* **38**, 1092-1104 (2013).
2. Ait-Oufella, H., Sage, A.P., Mallat, Z. & Tedgui, A. Adaptive (T and B cells) immunity and control by dendritic cells in atherosclerosis. *Circ Res* **114**, 1640-1660 (2014).
3. Sage, A.P. & Mallat, Z. Multiple potential roles for B cells in atherosclerosis. *Ann Med* **46**, 297-303 (2014).
4. Tsiantoulas, D., Sage, A.P., Mallat, Z. & Binder, C.J. Targeting B cells in atherosclerosis: closing the gap from bench to bedside. *Arterioscler Thromb Vasc Biol* **35**, 296-302 (2015).
5. Ait-Oufella, H.*, et al.* B cell depletion reduces the development of atherosclerosis in mice. *J Exp Med* **207**, 1579-1587 (2010).
6. Kyaw, T.*, et al.* Conventional B2 B cell depletion ameliorates whereas its adoptive transfer aggravates atherosclerosis. *J Immunol* **185**, 4410-4419 (2010).
7. Kyaw, T., Tipping, P., Bobik, A. & Toh, B.H. Protective role of natural IgM-producing B1a cells in atherosclerosis. *Trends Cardiovasc Med* **22**, 48-53 (2012).
8. Sage, A.P.*, et al.* BAFF receptor deficiency reduces the development of atherosclerosis in mice--brief report. *Arterioscler Thromb Vasc Biol* **32**, 1573-1576 (2012).

9. Candando, K.M., Lykken, J.M. & Tedder, T.F. B10 cell regulation of health and disease. *Immunol Rev* **259**, 259-272 (2014).

10. Rosser, E.C. & Mauri, C. Regulatory B cells: origin, phenotype, and function. *Immunity* **42**, 607-612 (2015).

11. Dang, V.D., Hilgenberg, E., Ries, S., Shen, P. & Fillatreau, S. From the regulatory functions of B cells to the identification of cytokine-producing plasma cell subsets. *Curr Opin Immunol* **28**, 77-83 (2014).

12. Sage, A.P.*, et al.* Regulatory B cell-specific interleukin-10 is dispensable for atherosclerosis development in mice. *Arterioscler Thromb Vasc Biol* **35**, 1770-1773 (2015).

13. Strom, A.C.*, et al.* B regulatory cells are increased in hypercholesterolaemic mice and protect from lesion development via IL-10. *Thromb Haemost* **114**, 835-847 (2015).

14. Pillai, S. & Cariappa, A. The follicular versus marginal zone B lymphocyte cell fate decision. *Nat Rev Immunol* **9**, 767-777 (2009).

15. Clement, M.*, et al.* Control of the T follicular helper-germinal center B-cell axis by CD8(+) regulatory T cells limits atherosclerosis and tertiary lymphoid organ development. *Circulation* **131**, 560-570 (2015).

16. Grasset, E.K.*, et al.* Sterile inflammation in the spleen during atherosclerosis provides oxidation-specific epitopes that induce a protective B-cell response. *Proc Natl Acad Sci U S A* **112**, E2030-2038 (2015).

17. Saito, T.*, et al.* Notch2 is preferentially expressed in mature B cells and indispensable for marginal zone B lineage development. *Immunity* **18**, 675-685 (2003).

18. Tanigaki, K.*, et al.* Notch-RBP-J signaling is involved in cell fate determination of marginal zone B cells. *Nat Immunol* **3**, 443-450 (2002).

19. Witt, C.M., Won, W.J., Hurez, V. & Klug, C.A. Notch2 haploinsufficiency results in diminished B1 B cells and a severe reduction in marginal zone B cells. *J Immunol* **171**, 2783-2788 (2003).

20. Gold, E.S.*, et al.* ATF3 protects against atherosclerosis by suppressing 25-hydroxycholesterol-induced lipid body formation. *J Exp Med* **209**, 807-817 (2012).

21. Gilchrist, M.*, et al.* Systems biology approaches identify ATF3 as a negative regulator of Toll-like receptor 4. *Nature* **441**, 173-178 (2006).

22. De Nardo, D.*, et al.* High-density lipoprotein mediates anti-inflammatory reprogramming of macrophages via the transcriptional regulator ATF3. *Nat Immunol* **15**, 152-160 (2014).

23. Hoetzenecker, W.*, et al.* ROS-induced ATF3 causes susceptibility to secondary infections during sepsis-associated immunosuppression. *Nat Med* **18**, 128-134 (2011).

24. Herieka, M. & Erridge, C. High-fat meal induced postprandial inflammation. *Mol Nutr Food Res* **58**, 136-146 (2014).

25. Good-Jacobson, K.L.*, et al.* PD-1 regulates germinal center B cell survival and the formation and affinity of long-lived plasma cells. *Nat Immunol* **11**, 535-542 (2010).

26. Cinamon, G., Zachariah, M.A., Lam, O.M., Foss, F.W., Jr. & Cyster, J.G. Follicular shuttling of marginal zone B cells facilitates antigen transport. *Nat Immunol* **9**, 54-62 (2008).

27. Pereira, J.P., Kelly, L.M. & Cyster, J.G. Finding the right niche: B-cell migration in the early phases of T-dependent antibody responses. *Int Immunol* **22**, 413-419 (2010).

28. Cyster, J.G., Dang, E.V., Reboldi, A. & Yi, T. 25-Hydroxycholesterols in innate and adaptive immunity. *Nat Rev Immunol* **14**, 731-743 (2014).

29. Ma, C.S., Deenick, E.K., Batten, M. & Tangye, S.G. The origins, function, and regulation of T follicular helper cells. *J Exp Med* **209**, 1241-1253 (2012).

30. Zinselmeyer, B.H.*, et al.* PD-1 promotes immune exhaustion by inducing antiviral T cell motility paralysis. *J Exp Med* **210**, 757-774 (2013).

31. Weill, J.C., Weller, S. & Reynaud, C.A. Human marginal zone B cells. *Annu Rev Immunol* **27**, 267-285 (2009).

32. Descatoire, M.*, et al.* Identification of a human splenic marginal zone B cell precursor with NOTCH2-dependent differentiation properties. *J Exp Med* **211**, 987-1000 (2014).

33. Zotos, D.*, et al.* IL-21 regulates germinal center B cell differentiation and proliferation through a B cell-intrinsic mechanism. *J Exp Med* **207**, 365-378 (2010).

34. Lee, J.Y., *et al.* The transcription factor KLF2 restrains CD4(+) T follicular helper cell differentiation. *Immunity* **42**, 252-264 (2015).

35. Moriyama, S., *et al.* Sphingosine-1-phosphate receptor 2 is critical for follicular helper T cell retention in germinal centers. *J Exp Med* **211**, 1297-1305 (2014).

36. Weber, J.P., *et al.* ICOS maintains the T follicular helper cell phenotype by down-regulating Kruppel-like factor 2. *J Exp Med* **212**, 217-233 (2015).

37. Kroenke, M.A., *et al.* Bcl6 and Maf cooperate to instruct human follicular helper CD4 T cell differentiation. *J Immunol* **188**, 3734-3744 (2012).

38. Liu, X., *et al.* Transcription factor achaete-scute homologue 2 initiates follicular T-helper-cell development. *Nature* **507**, 513-518 (2014).

39. Choi, Y.S., *et al.* ICOS receptor instructs T follicular helper cell versus effector cell differentiation via induction of the transcriptional repressor Bcl6. *Immunity* **34**, 932-946 (2011).

40. Soh, S.Y., *et al.* NKT Cell Hyporesponsiveness Leads to Unrestrained Accumulation of Marginal Zone B Cells in Hypercholesterolemic Apolipoprotein E-Deficient Mice. *J Immunol* **197**, 3894-3904 (2016).

41. Rosser, E.C., *et al.* Regulatory B cells are induced by gut microbiota-driven interleukin-1beta and interleukin-6 production. *Nat Med* **20**, 1334-1339 (2014).

42. Bankovich, A.J., Shiow, L.R. & Cyster, J.G. CD69 suppresses sphingosine 1-phosophate receptor-1 (S1P1) function through interaction with membrane helix 4. *J Biol Chem* **285**, 22328-22337 (2010).

43. Hannedouche, S., *et al.* Oxysterols direct immune cell migration via EBI2. *Nature* **475**, 524-527 (2011).

44. Liu, C.*, et al.* Oxysterols direct B-cell migration through EBI2. *Nature* **475**, 519-523 (2011).

45. Xu, H.*, et al.* Follicular T-helper cell recruitment governed by bystander B cells and ICOS-driven motility. *Nature* **496**, 523-527 (2013).

46. Gotsman, I.*, et al.* Proatherogenic immune responses are regulated by the PD-1/PD-L pathway in mice. *J Clin Invest* **117**, 2974-2982 (2007).

47. Bu, D.X.*, et al.* Impairment of the programmed cell death-1 pathway increases atherosclerotic lesion development and inflammation. *Arterioscler Thromb Vasc Biol* **31**, 1100-1107 (2011).

48. Khan, A.R.*, et al.* PD-L1hi B cells are critical regulators of humoral immunity. *Nat Commun* **6**, 5997 (2015).

49. Johnston, R.J.*, et al.* Bcl6 and Blimp-1 are reciprocal and antagonistic regulators of T follicular helper cell differentiation. *Science* **325**, 1006-1010 (2009).

50. Sage, P.T., Francisco, L.M., Carman, C.V. & Sharpe, A.H. The receptor PD-1 controls follicular regulatory T cells in the lymph nodes and blood. *Nat Immunol* **14**, 152-161 (2013).

FIGURE LEGENDS

Figure 1. Marginal zone B cells limit the development of atherosclerosis. *Ldlr*$^{-/-}$ mice were transplanted with donor bone marrow cells from *Cd79a*$^{Cre/+}$;*Rbpjk*$^{flox/flox}$ or *Cd79a*$^{+/;}$/*Rbpjk*$^{flox/flox}$ mice after consumption of a high cholesterol diet for 8 (a-b) or 16 (c) weeks. (a) Representative flow cytometry plots and total numbers of the indicated splenic B cell subsets by flow cytometry (n=9 mice per group). T2-MZP refers to transitional T2 and marginal zone progenitor B cells; T1 refers to transitional T1 B cells (see Methods). Data are presented as box-and-whisker plots. (b, c) Representative images of Masson trichrome staining and quantification of atherosclerotic plaque area in aortic roots (each symbol represents an individual mouse; horizontal bars denote mean ± s.e.m.). Original magnification, x10. Scale bars, 500 μm. For (a-c), two-tailed unpaired Student t-test or 2 way Anova * $p<0.05$; ** $p<0.01$ and *** $p<0.001$.

Figure 2. Marginal zone B cells limit the development of atherosclerosis through inhibition of the Tfh response. *Ldlr*$^{-/-}$ mice were transplanted with donor bone marrow cells from *Cd79a*$^{Cre/+}$;*Rbpjk*$^{flox/flox}$ or *Cd79a*$^{+/;}$/*Rbpjk*$^{flox/flox}$ mice after the consumption of a high cholesterol (a-d) diet for 8 weeks, with or without concomitant treatment with anti-CD4 (c) or anti-ICOSL (d) depleting antibodies. (**a**) Representative flow cytometry plots and percentage of CD44^{hi}CD62L^{-} T effector memory (TEM) and (**b**) Tfh (CD4^{+}CXCR5^{hi}PD1^{hi}) cells with respect to total CD4^{+} T cells (each symbol represents an individual mouse; horizontal bars denote mean ± s.e.m.). (c-d) Representative images of Masson trichrome staining and quantification of atherosclerotic plaque area in aortic roots (each symbol represents an individual mouse; horizontal bars denote mean ±

s.e.m.). Original magnification, x10. Scale bars, 500 μm. For (a-d) two-tailed unpaired Student t-test or 2 way Anova * $p<0.05$; ** $p<0.01$ and *** $p<0.001$.

Figure 3. High cholesterol diet activates a homeostatic and anti-inflammatory program in MZB cells. (a) Clustered heat map of 92 genes that were differentially expressed in splenic MZB cells subjected to RNA-seq analysis, comparing cells sorted from *Ldlr*$^{-/-}$ mice fed a chow or a high cholesterol diet for 8 weeks (see Methods). Each group contains samples from 5 independent mice. (b) qRT-PCR validation of selected genes that were differentially expressed in the RNA-seq analysis (each symbol represents an individual mouse and horizontal bars denote mean ± s.e.m.); these mice were different than the ones used for the RNA-seq analysis. (c) Significantly enriched ($P<0.01$; Fischer´s exact test) Ingenuity canonical pathways in the differentially-expressed genes. Bars represent log Benjamini-Honchberg adjusted P value. In brackets, the number of differentially expressed genes (RNAseq analysis) that belong to each signaling pathway. In bold, selected signaling pathways related to B cell function. (d) Schematic diagram of BCR and TLR signaling pathways and their overlap with critical regulatory genes that are differentially expressed in MZB cells from mice fed a chow or high cholesterol diet, based on the RNA-seq analysis. The color code represents fold-change expression values overlaid onto the pathways: blue indicates down-regulated and red indicates up-regulated genes. Diagram also indicates potential relevant activating ligands (OxLDL, CpG DNA) and cellular localization of each molecule or gene product.

Figure 4. ATF3 expression in MZB cells controls Tfh accumulation in response to high cholesterol diet and is required for the atheroprotective effect of MZB cells. Quantitative mRNA expression for *Il6* (a) and *Cd274* (b), and protein expression (mean fluorescence intensity, MFI) of PDL1 by flow cytometry (c), in sorted MZB cells (a,b) or total B cells (c) from WT or *Atf3*$^{-/-}$ mice treated with or without LPS (10 μg/mL) for 3 h (each symbol represents an individual mouse; horizontal bars denote mean ± s.e.m.). (d) Representative images of PDL1 (yellow) and IgM (magenta) immnostaining in spleen sections from *Ldlr*$^{-/-}$ mice transplanted with mixed BM containing 80% *Cd79a*$^{Cre/+}$;*Rbpjk*$^{flox/flox}$ BM plus 20% WT BM (WT MZB) or *Atf3*$^{-/-}$ BM (*Atf3*$^{-/-}$ MZB). BM from *Cd274*$^{-/-}$ mice was used as a negative control for PDL1 staining. White color indicates detection of PDL1 expression on IgM^{+} MZB cells. Original magnification, x40. Scale bars, 10 μm. (e) Quantitation of the percentage of PDL1-positive cells relative to total IgM-positive cells in the WT MZB and *Atf3*$^{-/-}$ MZB groups, as assessed by immunostaining. Each symbol represents an individual mouse; horizontal bars denote mean ± s.e.m. 100 MZB cells/mouse from at least 5 different sections were analyzed. (f-g) Percentages of splenic Tfh (f) and GC (g) cells in the No MZB (*Ldlr*$^{-/-}$ mice transplanted with BM containing 100% *Cd79a*$^{Cre/+}$;*Rbpjk*$^{flox/flox}$), WT MZB and *Atf3*$^{-/-}$ MZB groups**.**. (h) Representative images of Masson trichrome staining and quantification of atherosclerotic plaque area in aortic roots (each symbol represents an individual mouse; horizontal bars denote mean ± s.e.m.). Original magnification, x10. Scale bars, 500 μm. (i) Quantification of atherosclerotic plaque area in aortic arches from *en face* oil red O-stained aortas. For (a-i) two-tailed unpaired Student t-test * $p<0.05$; ** $p<0.01$ and *** $p<0.001$.

Figure 5. MZB cells limit Tfh motility and control the pro-atherogenic Tfh-GC response through upregulation of PDL1. (a, b) *Cd274* and *Icosl* mRNA expression in MZB (a) and (FOB) (b) cells sorted from *Ldlr*$^{-/-}$ mice fed a chow or high fat diet for 8 weeks (each symbol represents an individual mouse; horizontal bars denote mean ± s.e.m.). (c-e) Sorted Tfh cells were co-cultured with sorted MZB or FOB cells from NP_{18}-OVA and lipid A-immunized C57Bl6 mice fed a chow diet (see Methods). Tfh cell movement was visualized by time-lapse microscopy (see Methods) in presence or absence of anti-PDL1 in the co-culture. (c) Plots of x-y displacement (in μm) of individual cell traces, with the starting position realigned to the same origin. (d) Quantification of the T-cell centroid velocity (μm/min) and (e) contact time (s) between Tfh and MZB or FOB cells (each symbol represents one Tfh-B cell interaction and horizontal bars denote mean ± s.e.m.). (f-h) Percentages of Tfh cells (f) and GC B cells (g) in *Ldlr*$^{-/-}$ mice transplanted with mixed BM containing 80% *Cd79a*$^{Cre/+}$*;Rbpjk*$^{flox/flox}$ BM plus 20% WT BM (WT MZB) or *Cd274*$^{-/-}$ BM (*Cd274*$^{-/-}$ MZB); the mice consumed a HCD for 8 weeks. (h) Representative images of Masson trichrome staining and quantification of atherosclerotic plaque area in aortic roots (each symbol represents an individual mouse; horizontal bars denote mean ± s.e.m.). Original magnification, x10. Scale bars, 500 μm. For (a-h) two-tailed unpaired Student t-test * $p<0.05$; ** $p<0.01$ and *** $p<0.001$.

Figure 6. MZB cells control the Tfh program during atherosclerosis. (a) Clustered heat map of 109 genes that were differentially expressed in splenic Tfh cells subjected to

RNA-seq analysis, comparing cells sorted from *Ldlr*$^{-/-}$ mice transplanted with *Cd79a*$^{Cre/+}$/*Rbpjk*$^{flox/flox}$ BM or with *Cd79a*$^{+/+}$/*Rbpjk*$^{flox/flox}$ BM and fed a high cholesterol diet for 8 weeks (see Methods). Each group contains biological samples from 4 independent mice. (b) qRT-PCR validation of selected genes that were differentially expressed in the RNA-seq analysis. Each symbol represents an individual mouse; horizontal bars denote mean ± s.e.m. These mice were different than the ones used for the RNA-seq analysis. (c) Significantly enriched (P<0.01; Fischer´s exact test) Ingenuity canonical pathways in the differentially-expressed genes. Bars represent log Benjamini-Honchberg adjusted P value. In brackets, the number of differentially expressed genes (RNAseq analysis) that belong to each signaling pathway. In bold, selected signaling pathways related to T cell function. (d) Schematic diagram showing critical Tfh regulatory genes that are differentially expressed in the RNA-seq analysis. The color code represents the fold-change values overlaid onto the pathways: blue indicates down-regulated and red indicates up-regulated genes. Diagram also depicts the cell membrane.

MATERIALS AND METHODS

Animals. All experiments were approved by the Home Office, UK and were performed under PPL 80/2426. All mice were on a C57Bl/6 background. *Cd79a*$^{Cre/+}$, *Cxcr5*$^{-/-}$ and *Ldlr*$^{-/-}$ mice were originally from Jackson lab. *Rbpjk*$^{flox/flox}$ mice were kindly provided by Tasuku Honjo[18]; and *Cd274*$^{-/-}$ and *Atf3*$^{-/-}$ mice have been described[51,52]. *Cd79a*$^{Cre/+}$ were crossed with *Rbpjk*$^{flox/flox}$ to generate *Cd79a*$^{Cre/+}$/*Rbpjk*$^{flox/flox}$ and *Cd79a*$^{+/+}$/*Rbpjk*$^{flox/flox}$ littermate mice. To study the role of MZB cells in atherosclerosis, 6-8-week-old *Ldlr*$^{-/-}$ male mice were lethally irradiated and injected i.v. with bone marrow from

Cd79a$^{Cre/+}$/*Rbpjk*$^{flox/flox}$ or *Cd79a*$^{+/+}$/*Rbpjk*$^{flox/flox}$ mice. *Ldlr*$^{-/-}$ mice were randomly assigned to different experimental groups based on their weight at the beginning of the experiment. For some experiments, mixed BM containing 80% *Cd79a*$^{Cre/+}$/*Rbpjk*$^{flox/flox}$ BM plus 20% WT BM (for rescue experiments), 20% *Cd274*$^{-/-}$ BM or 20% *Atf3*$^{-/-}$ BM was injected. After 4 weeks recovery, mice were started on HCD (21% fat, 0.15% cholesterol) for 8 weeks. For depletion of CD4^{+} T or Tfh cells, mice received i.p. injections of purified neutralizing anti-CD4 (clone YTS 191.1, BioXCell) specific antibody (100 μg/mouse, every 10 days) or anti-ICOSL antibody (clone HK5.3, BioXCell) or isotype control (BioXCell) (100 g/mouse weekly).

Flow cytometry. Single cell suspensions of bone marrow, spleen, lymph node, blood and peritoneal lavage were stained with fluorophore-conjugated antibodies (Supplemental Table 1) and analyzed using LSRII Fortessa (BD) or FACSCantoII (BD) flow cytometers. Dead cells were excluded based on FSc and SSc. B cells were identified as B220^{+} IgM^{+} or CD19^{+} lymphocytes, MZB cells as CD23$^{lo/neg}$CD21^{hi}, FOB cells as CD23^{hi}CD21$^{lo/neg}$, T1 cells as CD23^{-}CD21^{-} and T2-MZP as CD23^{hi}CD21^{hi}; T cells were identified as CD3+ and either CD4^{+} or CD8^{+}, Th1 cells as T-bet^{+}, Th2 cells as GATA3^{+}, Th17 cells as RORγt^{+} and Tfh cells as CD4^{+} PD1^{hi} CXCR5^{hi} ICOS^{+}. Number of Tfh cells gated on CD4^{+} CXCR5^{hi} PD1 ^{hi} BCL6^{+} Foxp3^{-} revealed a high correlation (r^2=0.99) with the number of Tfh cells gated on CD4^{+} CXCR5 ^{hi} PD1 ^{hi} cells (data not shown). Germinal centre (GC) B cells were identified as CD19^{+} GL7^{hi} and CD95^{hi} cells. Monocytes were identified as CD11b^{+} and Ly6C$^{hi/lo}$ cells, neutrophils as Ly6G^{+} cells and macrophages as F4/80^{+} cells.

Extent and composition of atherosclerotic lesions. The lesions in the root of the aorta beneath all three-valve leaflets were analyzed. To measure atherosclerotic plaque size, we stained paraffin-embeded sections with Masson Trichrome. To characterize atherosclerotic lesion composition, we stained sections for macrophages (Mac-3, 1:200, clone M3/84, Santa Cruz), T cells (polyclonal CD3, 1:100, Dako, A0452). We performed each staining on a single slide (3 sections for each staining) from the same level of the aortic root for all experimental and control mice. Computer-assisted analysis (Image-J) was used to determine lesion size. The areas of specific cell types in the aortic cross-sections from the same experiment were quantified by the same blinded observer to minimize variations. All measurements were performed by manual selection of stained pixel thresholds and presented as percent positive (stained) area to the entire intimal area. $CD4^+$ T cells were counted and the data are presented as the number of T cells per total number of cells (DAPI) in atherosclerotic plaques. Whole aortas were used in an *en face* preparation for oil red O staining to measure aortic lipid deposition (considered as a measure of lesion size). Quantification was performed with J-Microvision.

Measurement of circulating antibodies. Specific antibody titers to given antigens in plasma were determined by chemiluminescent ELISA, as previously described[53, 54].

Measurement of serum lipid levels. Total cholesterol and HDL-C were measured using an enzymatic method in a Siemens Dimensions RxL analyzer according to the manufacturer's instructions.

Purification of MZB, FOB and Tfh cells. Single spleen cell suspensions were prepared by dissociation through 70 μm filters using a syringe plunger. For MZB and FOB cell purification, B cell enriched populations were first separated by autoMACS® Pro Separator (Miltenyi Biotech) using a B cell purification kit (Miltenyi Biotech) according to manufacturer´s instructions. B cells were then stained for 15 min at 4ºC with anti-CD23-PE and anti-CD21-FITC. After washing and staining with 7-AAD for cell viability, MZB ($CD21^{hi}CD23^{low}$) and FOB ($CD23^{hi}CD21^{low}$) cells were sorted using AriaIII Cell, Influx or FACSJazz sorters (BD). The purity of both cell populations was higher than 95%. For Tfh cell purification, T cell enriched cell suspensions were separated by autoMACS® Pro Separator using a T cell purification kit (Miltenyi Biotech) according to manufacturer´s instructions. T cells were then stained for 15 min at 4ºC with anti-CD4-PECy7 and anti-CXCR5-PE. After washing and staining for 7-AAD to determine cell viability, Tfh cells ($CD4^{+}CXCR5^{hi}$) were sorted (purity >95%).

Purification of human blood B cells. Anonymized apheresis cones with 10 mL of total blood were obtained from the Cambridge Blood Donor Centre in Addenbrooke´s Hospital. No further ethics approvals were requested to use the anonymized blood samples. PBMCs were isolated after density gradient centrifugation using Lymphoprep (Stemcell Technologies). B cells were then purified using a Miltenyi Human B cell purification kit for autoMACS® Pro Separator (Miltenyi Biotech). Naïve B cells were defined as $CD19^{pos}$ $CD27^{neg}$ and IgM^{neg}; and MZB like cells were defined as $CD19^{pos}$ $CD27^{pos}$ IgM^{pos} IgD^{pos} $CD21^{pos}$ and $CD1c^{pos}$ (all from Biolegend).

Human spleen B cells. Adult spleen samples were obtained from 4 organ donors (18, 19, 32, and 58 years old) with the authorization of the Agence de la Biomédecine, France (research protocol N° PF07-009). Informed consent was obtained for all patients. Spleen mononuclear cells were prepared from mechanically disrupted spleen samples after density gradient centrifugation on Ficoll-Paque PLUS (GE Healthcare). Staining was performed by incubating human splenocytes with the following antibodies: APC anti-CD27, APC-H7 anti-CD19, PE-Cy7 anti-CD274 (all from BD Biosciences) and FITC anti-IgD (Invitrogen). Dead cells were excluded using Sytox Blue staining (Life technologies). Flow cytometric data acquisition was done with a FACSCantoII instrument, and the data were analyzed with Diva (BD Biosciences) software.

BCR stimulation. Purified mouse B cells or sorted MZB and FOB cells were stimulated for 30 min, 3 hours or 6 hours with the F(ab)2 fragment of anti-IgM (eBioscience) (10 ug/mL). Purified human B cells were cultured for 18 hours in pre-coated human anti-IgM (eBioscience) plates with soluble anti-CD40 (eBioscience). Ibrutinib, a phospho-Bruton´s tyrosine kinase (pBTK) inhibitor (Sellekchem) was used at 5 μM in DMSO. Control 'untreated' cells were incubated with the same final concentration of DMSO.

Tfh cell motility assay. C57Bl/6 mice were injected i.v. with OT-II CD4+ T cells from OT-II mice (Charles River). The following day, the mice were injected i.p. with NP_{18}-

OVA (Biosearch) and lipid A (Sigma-Aldrich). Mice were killed 8 days after injection and Tfh, MZB and FOB cells were sorted. For HCD MZB cells, MZB were sorted from mice that had been on an HCD diet for 8 weeks. CFSE-labeled MZB or FOB cells (4 x 10^4) were co-cultured with Tfh cells (2 x 10^5) in rmICAM-1-Fc Chimera coated chambered coverglass (LAB-TEK®, NUNC). First, MZB or FOB cells were cultured for 10 min with or without anti-PDL1 blocking antibody, and then the Tfh cells were added for another 10 min before starting imaging. Images were acquired using a Zeiss LSM710 confocal microscope (20X lens) every 10 seconds for 20 minutes. To track cell motility, we used Volocity software (Improvision). T-cell/MZB-FOB interactions were then monitored by ImageJ Version 1.49 software.

RNA sequencing. RNA was isolated from sorted MZB or Tfh cells using the mirVAna isolation kit (Ambion). The quality of the RNA extracted was checked using a Bioanalyser RNA Pico kit (Agilent) with RIN values > 7. RNA (2.5 ng) was whole transcriptome-amplified using the Ovation RNA-seq System V2 (NuGEN). To prepare the RNA-seq library, the amplified cDNA (2µg per sample) was fragmented to 200 bp using a Bioruptor Sonicator (Diagenode), and barcode ligation and end repair were performed using the Ovation Rapid DR Library System (NuGEN). The barcoded libraries were combined and loaded onto an Illumina HiSeq 2500 system for single end 50 bp sequencing at the Genomics Core Facility, Cambridge Institute, CRUK. The sequencing yielded 213 million reads and the reads were aligned onto the mouse GRCm38 genome using Tophat 2.0.11[55]; the average mapping rate was 93.5%. Gene abundance and differential expression were determined with Cufflinks 2.2.1[56] and expressed in

fragments per kilobase per million of mapped reads (FPKM). Genes with a linear fold change of > 1.5 fold in FPKM and a Benjamini Hochberg False Discovery Rate < 10% were considered to be differentially expressed.

Quantitative real time polymerase chain reaction. For gene expression analysis, RNA from sorted MZB, FOB and Tfh cells was isolated using an RNAeasy mini kit (Qiagen). RT-PCR was performed using a QuantiTect Reverse transcription kit (Qiagen) or a Quantitect Whole transcriptome kit depending on the yield of mRNA. qRT-PCR was performed with SYBR-green primers. Primers sequences are listed in Table 2S.

Statistical analysis. Values are expressed as means ± s.e.m. Based on pilot experiments, we found that MZB deficiency increases lesion size by 2-fold. Use of the equation for Student's t test for the difference of 2 means gives n=6 for detection of a 50% increase in lesion size with α=0.05 and 90% power. Where data sets passed normality tests, differences between values were examined using the parametric two-tailed unpaired Student t-test or two-way ANOVA; other data sets were examined using the non-parametric Mann Whitney U test, and were considered significant at $P<0.05$. Hypergeometric enrichment analysis of canonical pathways within the differentially regulated gene set was carried out using Ingenuity Pathway Analysis (Qiagen, Redwood City, CA, USA).

Methods only references

18. Tanigaki, K., *et al*. Notch-RBP-J signaling is involved in cell fate determination of marginal zone B cells. *Nat Immunol* **3**, 443-450 (2002).

51. Dong, H., *et al*. B7-H1 determines accumulation and deletion of intrahepatic CD8(+) T lymphocytes. *Immunity* **20**, 327-336 (2004).

52. Hartman, M.G., *et al*. Role for activating transcription factor 3 in stress-induced beta-cell apoptosis. *Mol Cell Biol* **24**, 5721-5732 (2004).

53. Binder, C.J.*, et al.* Pneumococcal vaccination decreases atherosclerotic lesion formation: molecular mimicry between Streptococcus pneumoniae and oxidized LDL. *Nat Med* **9**, 736-743 (2003).

54. Chou, M.Y.*, et al.* Oxidation-specific epitopes are dominant targets of innate natural antibodies in mice and humans. *J Clin Invest* **119**, 1335-1349 (2009).

55. Kim D, Pertea G, Trapnell C, Pimentel H, Kelley R, Salzberg SL. TopHat2: accurate alignment of transcriptomes in the presence of insertions, deletions and gene fusions. *Genome Biol* **14**, R36 (2013).

56. Trapnell C, Hendrickson DG, Sauvageau M, Goff L, Rinn JL, Pachter L. Differential analysis of gene regulation at transcript resolution with RNA-seq. *Nat Biotechnol* **31**, 46-53 (2013)

Editorial summary

Marginal zone B cells in the spleen suppress atherosclerosis in mice by dampening the proatherogenic T follicular helper response, via interaction of PDL1 on marginal zone B cells with PD1 on T follicular helper cells.

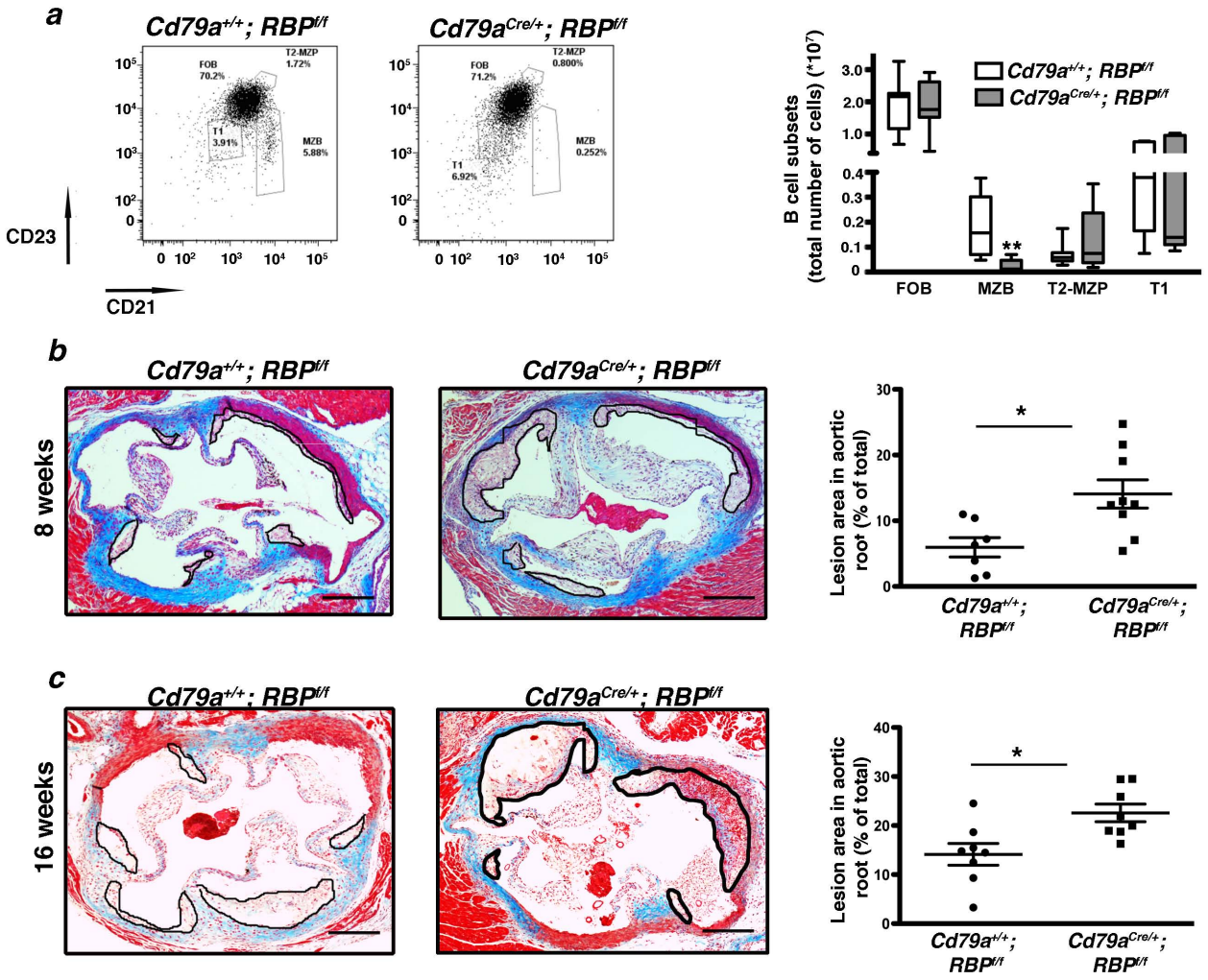
a
Cd79a+/+; RBPf/f
Cd79aCre/+; RBPf/f
FOB
70.2%
T2-MZP
1.72%
T1
3.91%
MZB
5.88%
FOB
71.2%
T2-MZP
0.800%
T1
6.92%
MZB
0.252%
CD23
CD21
B cell subsets
(total number of cells) (*10^7)
Cd79a+/+; RBPf/f
Cd79aCre/+; RBPf/f
**
FOB
MZB
T2-MZP
T1
b
8 weeks
Cd79a+/+; RBPf/f
Cd79aCre/+; RBPf/f
Lesion area in aortic root* (% of total)
*
Cd79a+/+; RBPf/f
Cd79aCre/+; RBPf/f
c
16 weeks
Cd79a+/+; RBPf/f
Cd79aCre/+; RBPf/f
Lesion area in aortic root (% of total)
*
Cd79a+/+; RBPf/f
Cd79aCre/+; RBPf/f

Figure 1

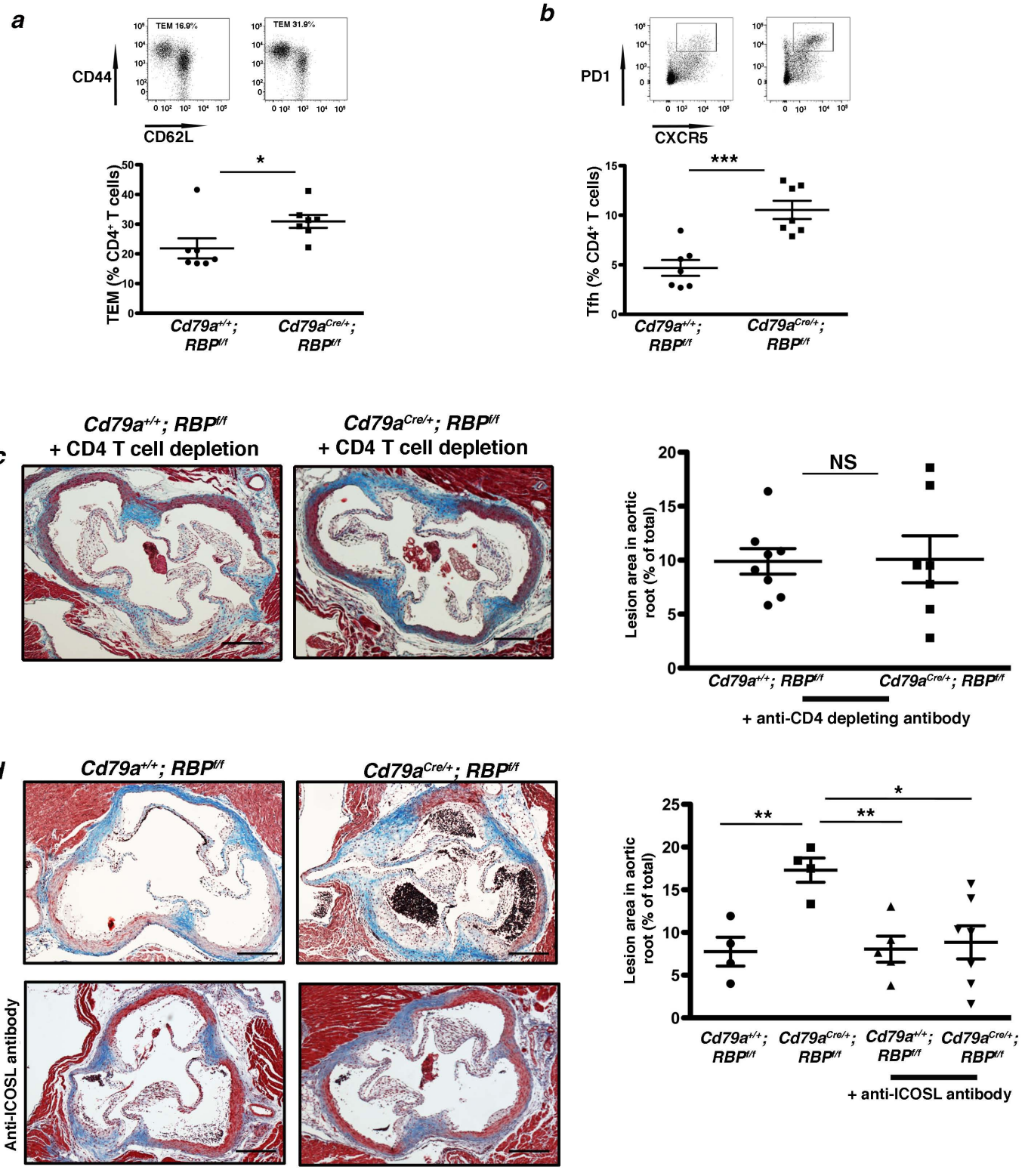
a
CD44
CD62L
TEM 16.9%
TEM 31.9%
TEM (% CD4+ T cells)
*
Cd79a+/+; RBPf/f
Cd79aCre/+; RBPf/f
b
PD1
CXCR5
Tfh (% CD4+ T cells)
***
c
Cd79a+/+; RBPf/f
+ CD4 T cell depletion
Cd79aCre/+; RBPf/f
+ CD4 T cell depletion
Lesion area in aortic root (% of total)
NS
+ anti-CD4 depleting antibody
d
Anti-ICOSL antibody
**
**
*
+ anti-ICOSL antibody

Figure 2

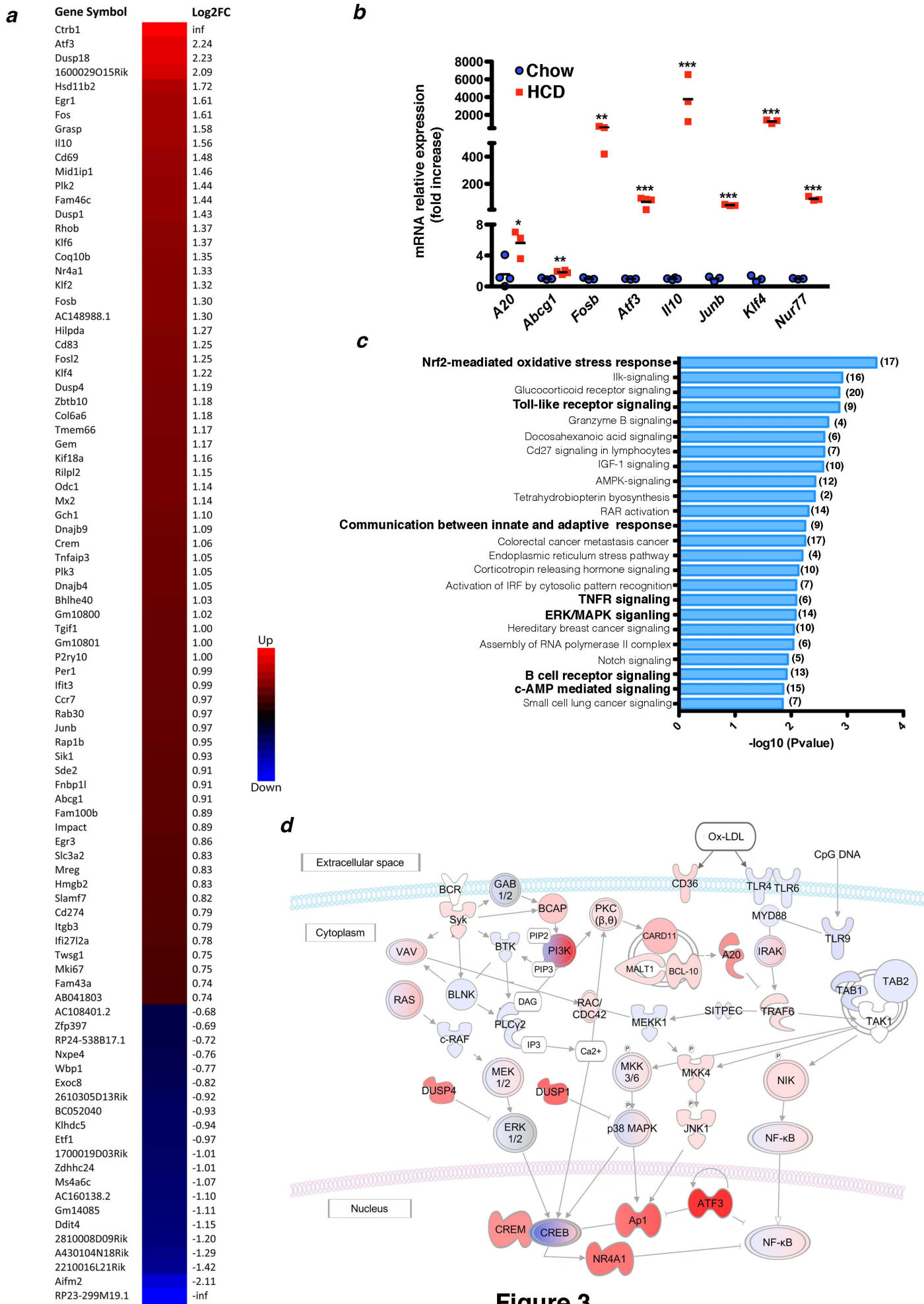
a
Gene Symbol
Log2FC
Ctrb1 inf
Atf3 2.24
Dusp18 2.23
1600029O15Rik 2.09
Hsd11b2 1.72
Egr1 1.61
Fos 1.61
Grasp 1.58
Il10 1.56
Cd69 1.48
Mid1ip1 1.46
Plk2 1.44
Fam46c 1.44
Dusp1 1.43
Rhob 1.37
Klf6 1.37
Coq10b 1.35
Nr4a1 1.33
Klf2 1.32
Fosb 1.30
AC148988.1 1.30
Hilpda 1.27
Cd83 1.25
Fosl2 1.25
Klf4 1.22
Dusp4 1.19
Zbtb10 1.18
Col6a6 1.18
Tmem66 1.17
Gem 1.17
Kif18a 1.16
Rilpl2 1.15
Odc1 1.14
Mx2 1.14
Gch1 1.10
Dnajb9 1.09
Crem 1.06
Tnfaip3 1.05
Plk3 1.05
Dnajb4 1.05
Bhlhe40 1.03
Gm10800 1.02
Tgif1 1.00
Gm10801 1.00
P2ry10 1.00
Per1 0.99
Ifit3 0.99
Ccr7 0.97
Rab30 0.97
Junb 0.97
Rap1b 0.95
Sik1 0.93
Sde2 0.91
Fnbp1l 0.91
Abcg1 0.91
Fam100b 0.89
Impact 0.89
Egr3 0.86
Slc3a2 0.83
Mreg 0.83
Hmgb2 0.83
Slamf7 0.82
Cd274 0.79
Itgb3 0.79
Ifi27l2a 0.78
Twsg1 0.75
Mki67 0.75
Fam43a 0.74
AB041803 0.74
AC108401.2 -0.68
Zfp397 -0.69
RP24-538B17.1 -0.72
Nxpe4 -0.76
Wbp1 -0.77
Exoc8 -0.82
2610305D13Rik -0.92
BC052040 -0.93
Klhdc5 -0.94
Etf1 -0.97
1700019D03Rik -1.01
Zdhhc24 -1.01
Ms4a6c -1.07
AC160138.2 -1.10
Gm14085 -1.11
Ddit4 -1.15
2810008D09Rik -1.20
A430104N18Rik -1.29
2210016L21Rik -1.42
Aifm2 -2.11
RP23-299M19.1 -inf
Gm14761 -inf
Up
Down
b
mRNA relative expression (fold increase)
Chow
HCD
A20
Abcg1
Fosb
Atf3
Il10
Junb
Klf4
Nur77
c
Nrf2-meadiated oxidative stress response (17)
Ilk-signaling (16)
Glucocorticoid receptor signaling (20)
Toll-like receptor signaling (9)
Granzyme B signaling (4)
Docosahexanoic acid signaling (6)
Cd27 signaling in lymphocytes (7)
IGF-1 signaling (10)
AMPK-signaling (12)
Tetrahydrobiopterin byosynthesis (2)
RAR activation (14)
Communication between innate and adaptive response (9)
Colorectal cancer metastasis cancer (17)
Endoplasmic reticulum stress pathway (4)
Corticotropin releasing hormone signaling (10)
Activation of IRF by cytosolic pattern recognition (7)
TNFR signaling (6)
ERK/MAPK siganling (14)
Hereditary breast cancer signaling (10)
Assembly of RNA polymerase II complex (6)
Notch signaling (5)
B cell receptor signaling (13)
c-AMP mediated signaling (15)
Small cell lung cancer signaling (7)
-log10 (Pvalue)
d
Extracellular space
Cytoplasm
Nucleus
Ox-LDL
CpG DNA
CD36
TLR4 TLR6
MYD88
TLR9
BCR
GAB 1/2
BCAP
Syk
PKC (β,θ)
CARD11
MALT1
BCL-10
A20
IRAK
TAB2
TAB1
TAK1
TRAF6
SITPEC
VAV
BTK
PIP2
PIP3
PI3K
RAS
BLNK
DAG
PLCγ2
IP3
Ca2+
RAC/ CDC42
MEKK1
c-RAF
MEK 1/2
ERK 1/2
MKK 3/6
MKK4
p38 MAPK
JNK1
NIK
NF-κB
DUSP4
DUSP1
CREM
CREB
Ap1
ATF3
NR4A1
NF-κB

Figure 3

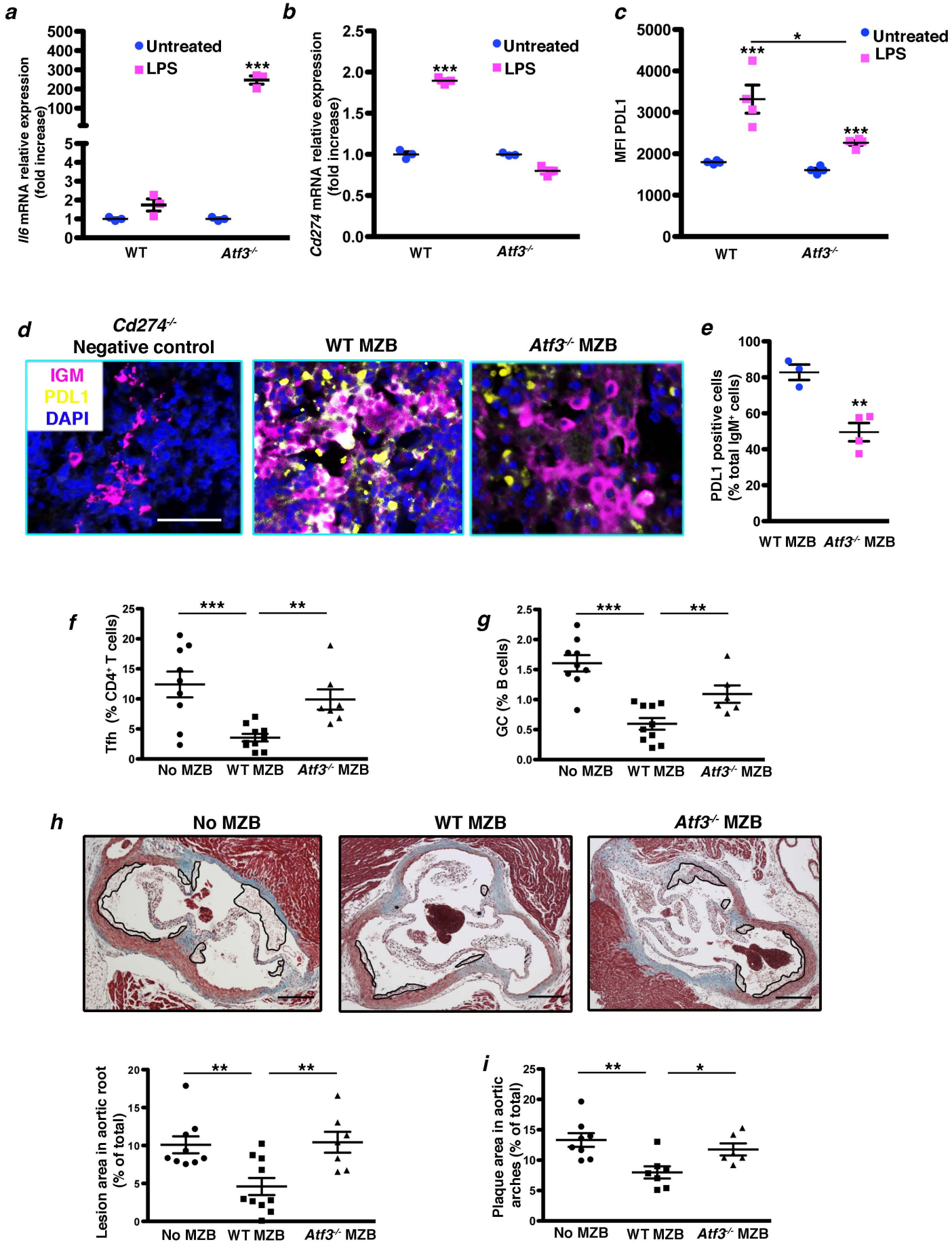
a
Il6 mRNA relative expression (fold increase)
Untreated
LPS
***
WT
Atf3-/-
b
Cd274 mRNA relative expression (fold increase)
Untreated
LPS
***
WT
Atf3-/-
c
MFI PDL1
Untreated
LPS
*
***
***
WT
Atf3-/-
d
Cd274-/-
Negative control
WT MZB
Atf3-/- MZB
IGM
PDL1
DAPI
e
PDL1 positive cells (% total IgM+ cells)
**
WT MZB
Atf3-/- MZB
f
Tfh (% CD4+ T cells)
***
**
No MZB
WT MZB
Atf3-/- MZB
g
GC (% B cells)
***
**
No MZB
WT MZB
Atf3-/- MZB
h
No MZB
WT MZB
Atf3-/- MZB
Lesion area in aortic root (% of total)
**
**
No MZB
WT MZB
Atf3-/- MZB
i
Plaque area in aortic arches (% of total)
**
*
No MZB
WT MZB
Atf3-/- MZB

Figure 4

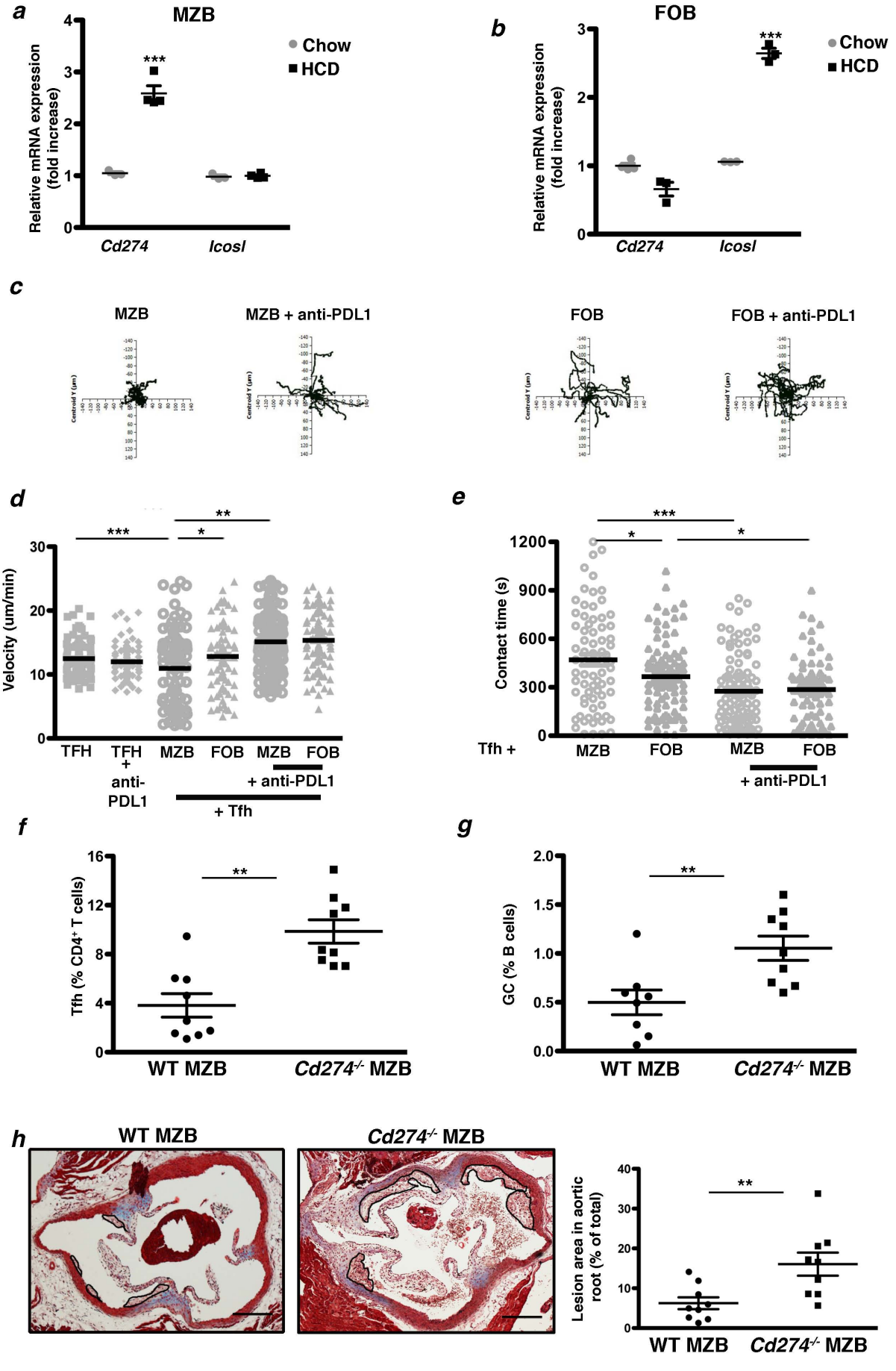
a
MZB
Relative mRNA expression (fold increase)
Chow
HCD
***
Cd274
Icosl
b
FOB
Relative mRNA expression (fold increase)
Chow
HCD
***
Cd274
Icosl
c
MZB
MZB + anti-PDL1
FOB
FOB + anti-PDL1
d
Velocity (um/min)
***
*
**
TFH
TFH + anti-PDL1
MZB
FOB
MZB + anti-PDL1
FOB + anti-PDL1
+ Tfh
e
Contact time (s)
***
*
*
Tfh +
MZB
FOB
MZB + anti-PDL1
FOB + anti-PDL1
f
Tfh (% CD4+ T cells)
**
WT MZB
Cd274-/- MZB
g
GC (% B cells)
**
WT MZB
Cd274-/- MZB
h
WT MZB
Cd274-/- MZB
Lesion area in aortic root (% of total)
**
WT MZB
Cd274-/- MZB

Figure 5

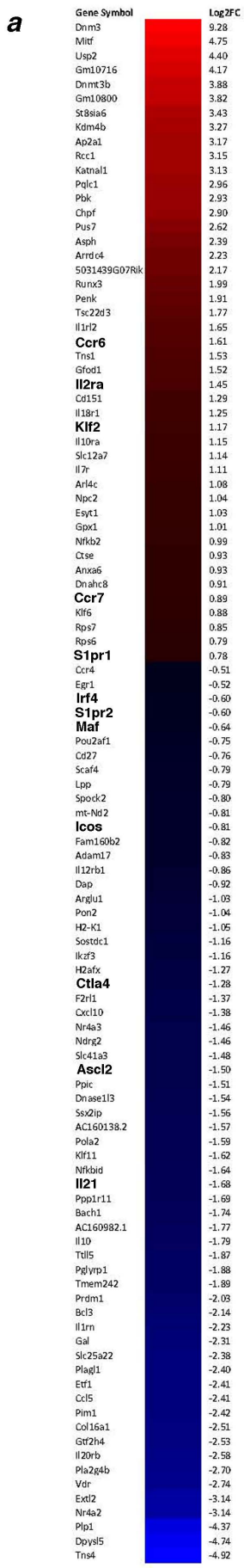

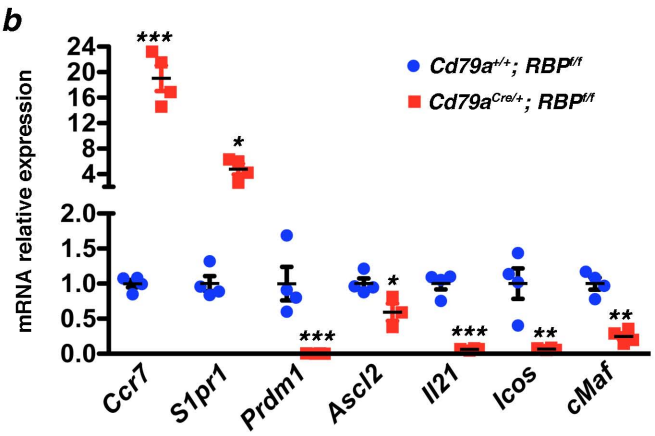

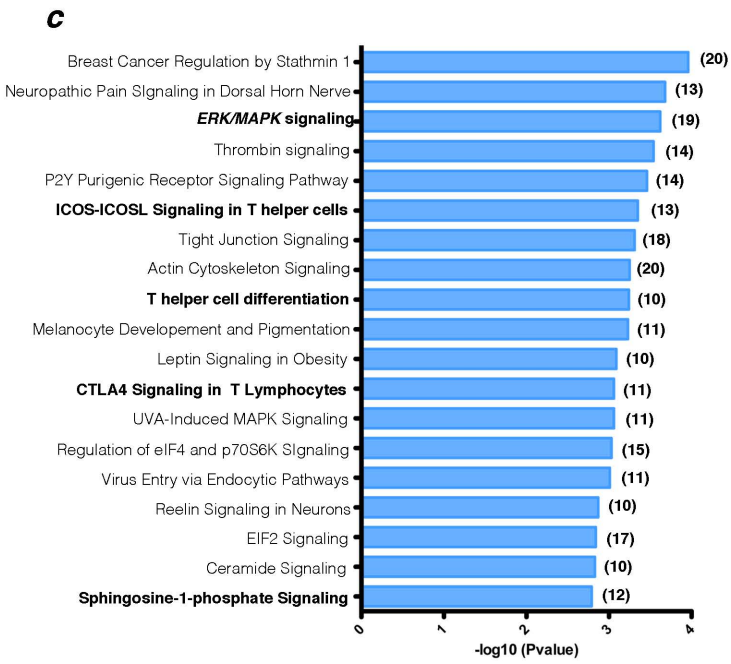

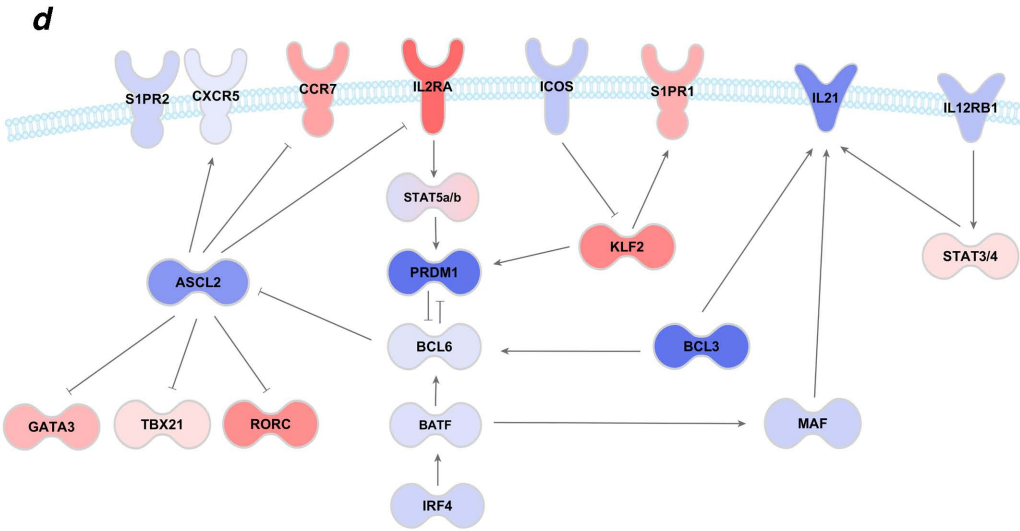

Positive regulators of TFH: Icos, Bcl6, Il21, Ascl2, Maf, etc
Negative regulators of TFH: Klf2, S1pr1, etc.

Figure 6

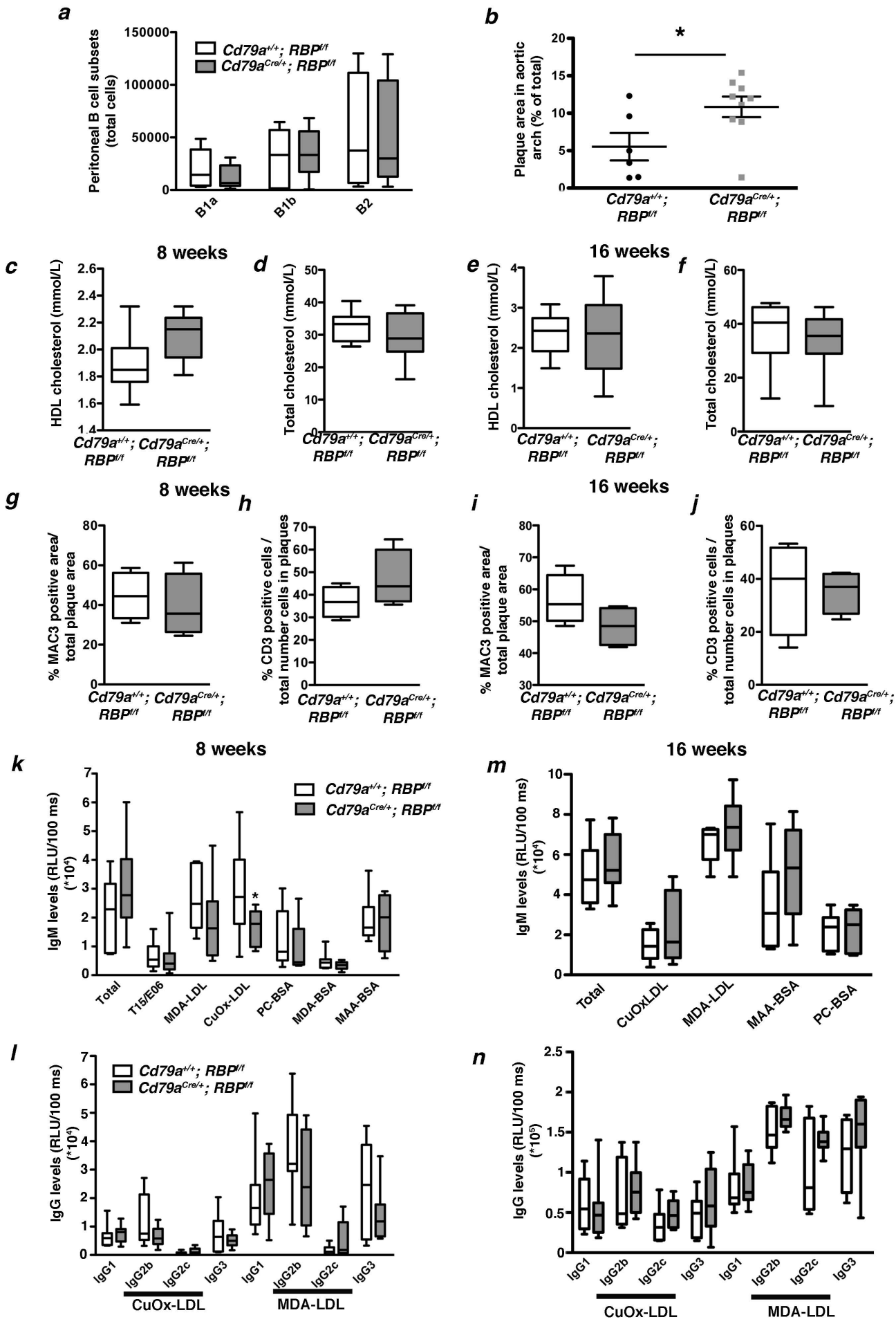
a
Peritoneal B cell subsets (total cells)
150000
100000
50000
0
Cd79a+/+; RBPf/f
Cd79aCre/+; RBPf/f
B1a
B1b
B2
b
Plaque area in aortic arch (% of total)
20
15
10
5
0
*
Cd79a+/+; RBPf/f
Cd79aCre/+; RBPf/f
8 weeks
16 weeks
c
HDL cholesterol (mmol/L)
2.6
2.4
2.2
2.0
1.8
1.6
1.4
d
Total cholesterol (mmol/L)
50
40
30
20
10
0
e
HDL cholesterol (mmol/L)
4
3
2
1
0
f
Total cholesterol (mmol/L)
60
40
20
0
Cd79a+/+; RBPf/f
Cd79aCre/+; RBPf/f
g
% MAC3 positive area/ total plaque area
80
60
40
20
0
h
% CD3 positive cells / total number cells in plaques
70
60
50
40
30
20
10
0
i
% MAC3 positive area/ total plaque area
80
70
60
50
40
30
j
% CD3 positive cells / total number cells in plaques
60
40
20
0
k
IgM levels (RLU/100 ms) (*10⁴)
7
6
5
4
3
2
1
0
*
Total
T15/E06
MDA-LDL
CuOx-LDL
PC-BSA
MDA-BSA
MAA-BSA
m
IgM levels (RLU/100 ms) (*10⁴)
10
8
6
4
2
0
Total
CuOxLDL
MDA-LDL
MAA-BSA
PC-BSA
l
IgG levels (RLU/100 ms) (*10⁴)
7
6
5
4
3
2
1
0
IgG1
IgG2b
IgG2c
IgG3
CuOx-LDL
MDA-LDL
n
IgG levels (RLU/100 ms) (*10⁵)
2.5
2
1.5
1
0.5
0
IgG1
IgG2b
IgG2c
IgG3
CuOx-LDL
MDA-LDL

Supplementary Figure 1. Further characterization of Ldlr-/- mice transplanted with wild type or MZB deficient bone marrow. *Ldlr*$^{-/-}$ mice were transplanted with donor bone marrow cells from *Cd79a*$^{Cre/+}$/*Rbpjk*$^{flox/flox}$ or *Cd79a*$^{+/+}$/*Rbpjk*$^{flox/flox}$ after the consumption of a high cholesterol diet for 8 weeks (a-d, g, h, k, l) or 16 weeks (e, f, i, j, m, n). (a) Total number of peritoneal B cell subsets by flow cytometry (n=7 to 9 mice per group). (b) Quantification of Oil red *en face* staining of aortic arches (with each symbol representing one animal and horizontal bars mean ± s.e.m.). Aortic arch was not available for quantification in one mouse in the WT group. HDL-C (c, e) and total cholesterol (d, f) levels in serum. Quantification of Mac3 (g, i) and CD3 (h, j) positive staining in atherosclerotic plaques (n=4 mice/group and 3 representative sections from each mouse were analyzed). Graphs showing total plasma and subtypes of IgM (k, m) and IgG (m, n) levels. In (k-m) n=7 and n=9 for each group at 8 weeks and n=8 for each group at 16 weeks. Whisker bars represents maximum and minimum levels. For (a-n) * $p<0.05$; ** $p<0.01$ and *** $p<0.001$. Student t-test.

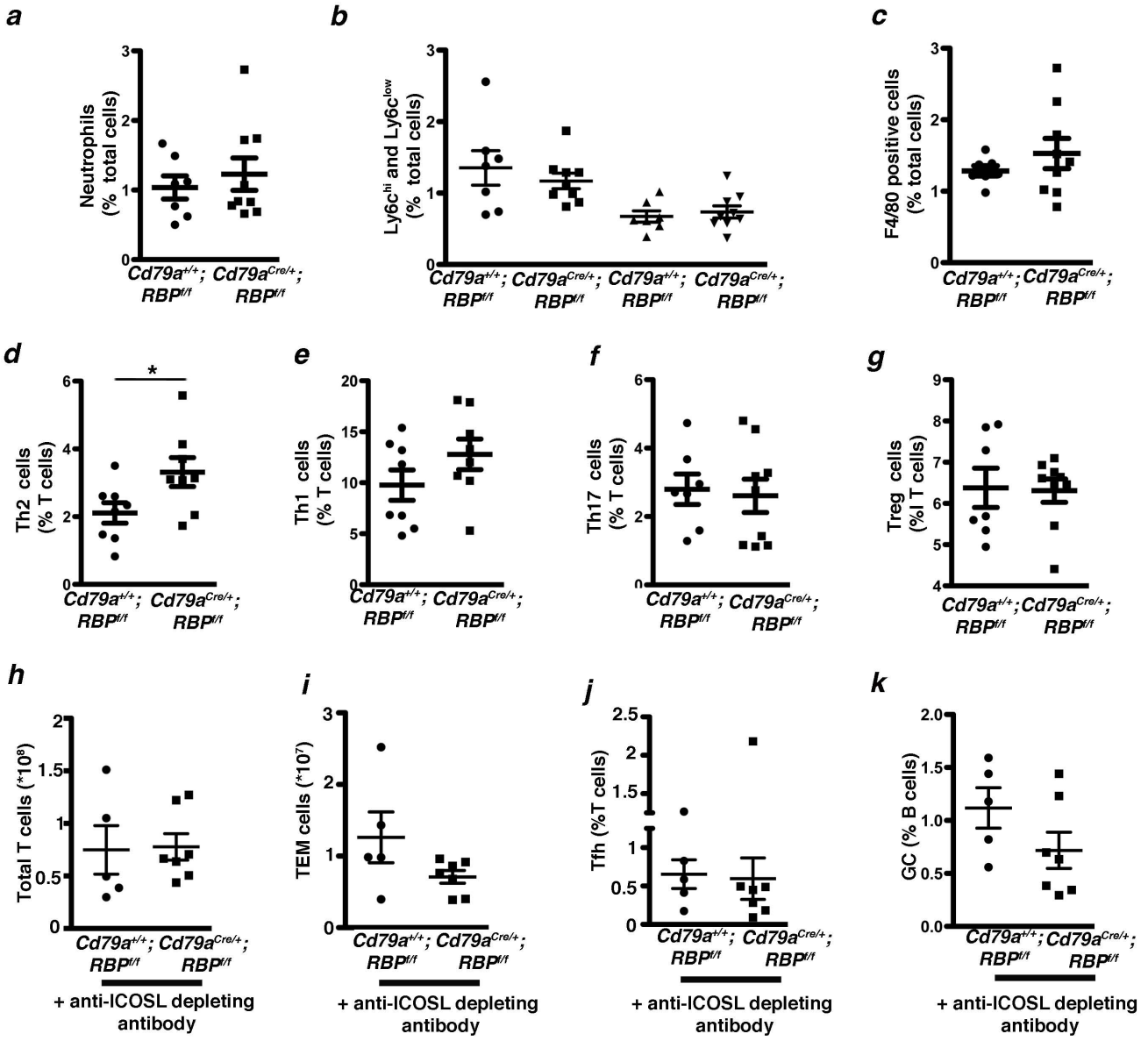

Supplementary Figure 2. Immune cell analyses on Ldlr-/- mice transplanted with wild type or MZB deficient bone marrow. *Ldlr*$^{-/-}$ mice were transplanted with donor bone marrow cells from *Cd79a*$^{Cre/+}$*/Rbpjk*$^{flox/flox}$ *vs. Cd79a*$^{+/+}$*/Rbpjk*$^{flox/flox}$ (a-k) or *Cd79a*$^{Cre/+}$*vs. Cd79a*$^{+/+}$ after the consumption of a high cholesterol diet for 8 weeks without treatment (a-g) or following 8 weeks of treatment with anti-ICOSL depleting antibody (h-k). Percentage of Ly6G positive (neutrophils) (a), Ly6C high and low (monocytes) (b) and F4/80 positive (macrophages) cells (c) with respect to total spleen cells. Percentage of T-bet (Th1) (d), GATA3 (Th2) (e), RORγt (Th17) (f) and FOXP3 (Treg) (g) positive cells in spleens, with respect to total T cells. (h) Total numbers of T cells, (i) T effector memory (TEM) cells and percentage of (j) Tfh cells and (k) GC B cells in spleen after the consumption of HCD for 8 weeks. Each symbol represents an individual mouse; horizontal bars denote mean ± s.e.m. For (a-k) two-tailed unpaired Student t-test or 2 way Anova * $p<0.05$; ** $p<0.01$ and *** $p<0.001$.

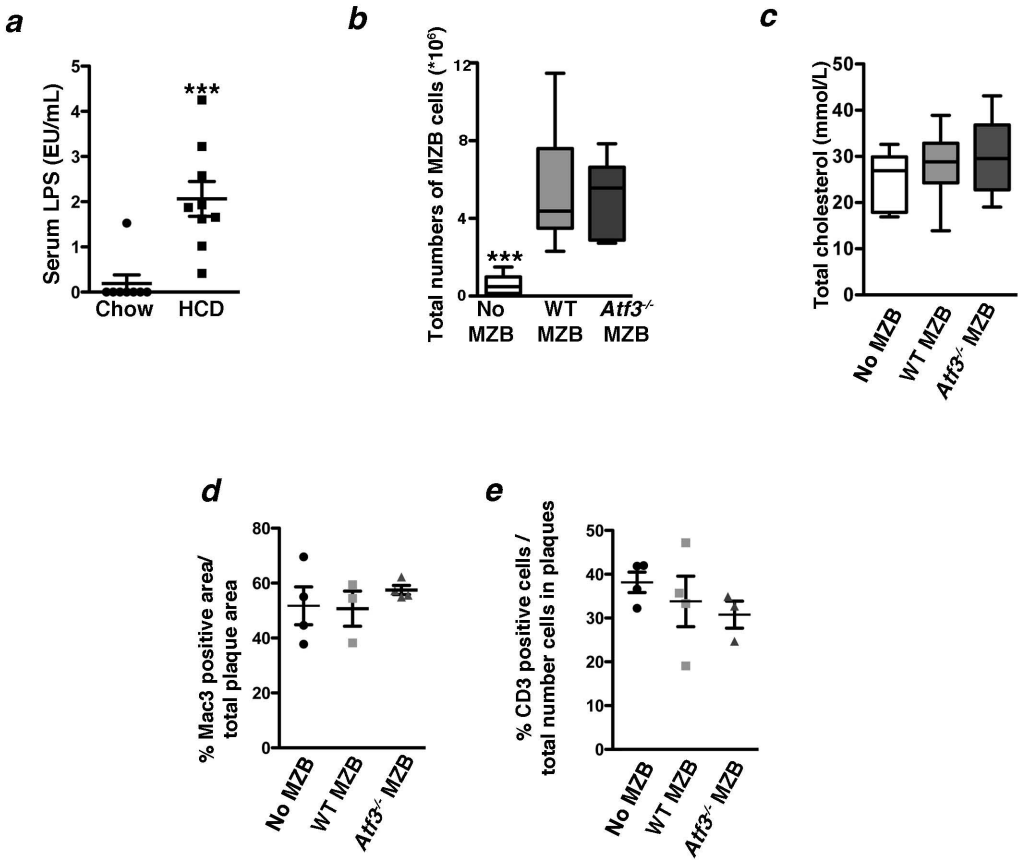

Supplementary Figure 3. Further characterization of Ldlr-/- mice with no MZB cells, wild type MZB cells or Atf3 deficient MZB cells. (a) LPS serum levels in mice after the consumption of a control chow *vs* high cholesterol diet for 8 weeks in $LDLr^{-/-}$ mice. Each symbol represents an individual mouse; horizontal bars denote mean ± s.e.m. (b-e) $Ldlr^{-/-}$ mice were transplanted with a mixed BM chimera containing 80% $Cd79a^{Cre/+}/Rbpjk^{flox/flox}$ + 20% WT (for rescue experiments) or $Atf3^{-/-}$ bone marrow ($Atf3^{-/-}$ MZB) (b-e). (b) Numbers of MZB cells in the spleens of the 3 groups of mice after BM transplantation and HCD for 8 weeks. (c) Total plasma cholesterol levels (n=7 to 10 in each group). Whisker bars represents maximum and minimum levels. Quantification of Mac3 (d) and CD3 (e) positive staining in atherosclerotic plaques of aortic roots. (Each dot represent a mouse and 3 representative sections from each mouse were analyzed). Horizontal bars represent mean ± s.e.m. For (a-e) * $p<0.05$; ** $p<0.01$ and *** $p<0.001$.

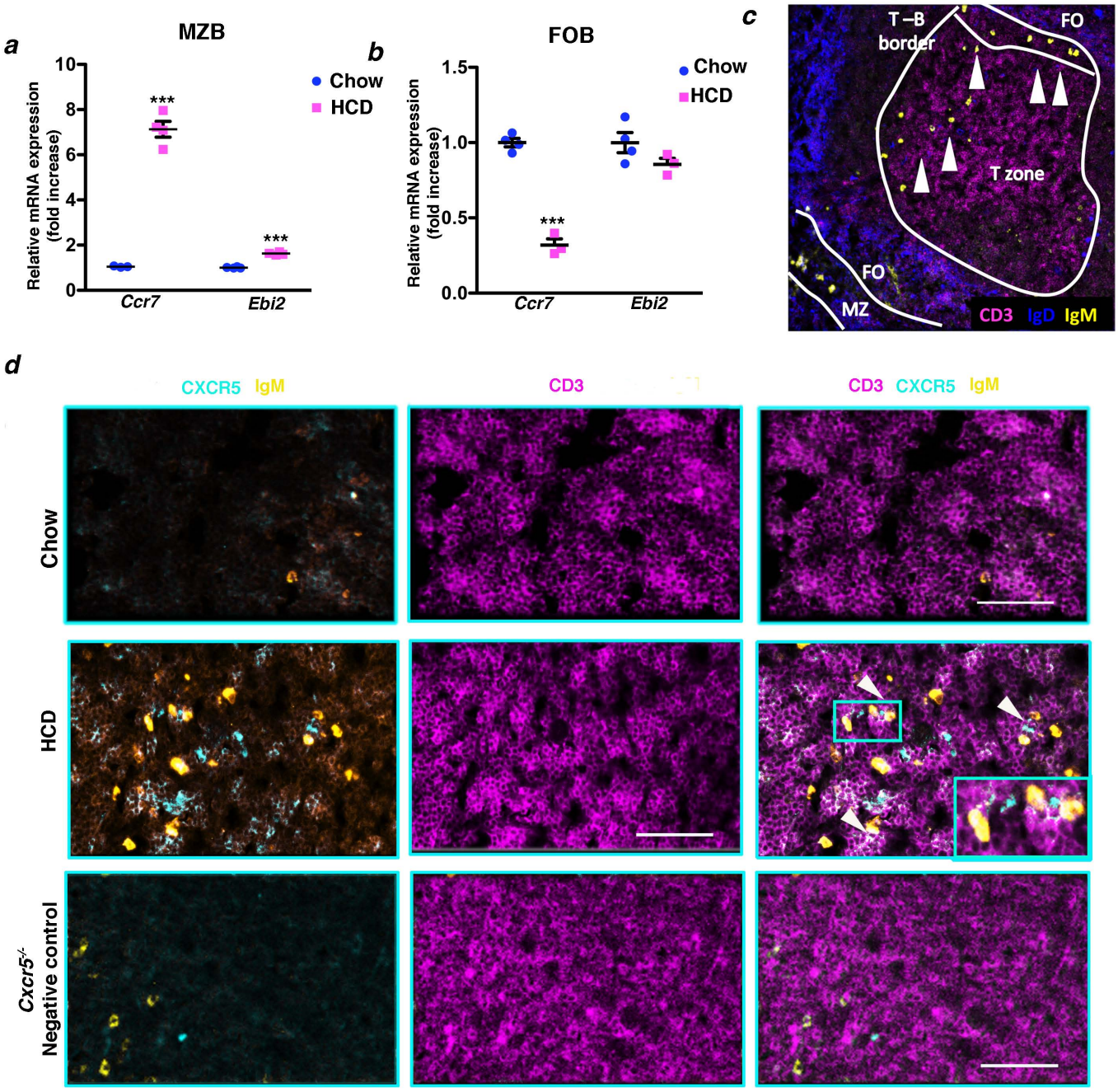

Supplementary Figure 4. Chemokine receptor expression and distribution of MZB cells in the spleen after high cholesterol diet. Relative mRNA expression for *Ccr7* and *Ebi2* on sorted MZB (a) and FOB (b) from *Ldlr*$^{-/-}$ mice after the consumption of chow diet or HCD (with each symbol representing one animal and horizontal bars mean ± s.e.m.). Two-tailed unpaired Student t-test * $p<0.05$; ** $p<0.01$ and *** $p<0.001$. (c) Representative spleen sections from *Ldlr*$^{-/-}$ mice after 8 weeks on chow diet or HCD showing T cell zone boundary. TFH cells (white) stained with CD3 (magenta) and CXCR5 (cyan) and MZB cells stained with IgM (yellow) in the T cell zone. A negative control for CXCR5 staining is shown (*Cxcr5*$^{-/-}$ mouse). Original magnification, 10x. Scale bars, 50 μm.

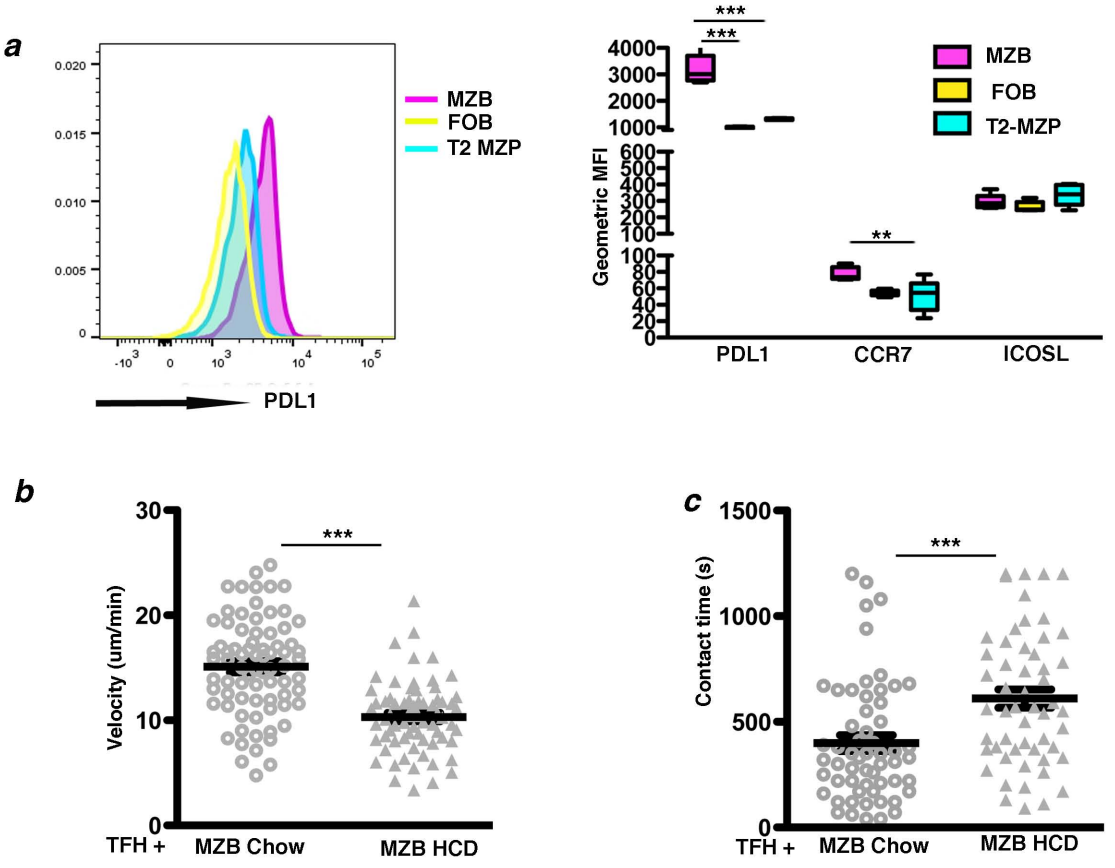

Supplementary Figure 5. Expression of PDL1 on splenic B cell subsets and effects of high cholesteriol diet on the interaction betwwen MZB cells and follicular helper T cells. (a) Diagram and quantification of surface PDL1, CCR7 and ICOSL expression by flow cytometry in FOB, MZB cells and MZ progenitors (MZP). (b, c) Labeled sorted MZB cells from mice fed a chow or a HCD for 8 weeks, co-cultured with sorted Tfh cells from previously immunized mice fed a chow diet. Tfh movement was visualized by time-lapse microscopy. (b) Quantification of the T-cell centroid velocity (μm/min) and (c) contact time (s) between B-Tfh cells (with each symbol representing one Tfh-B cell interaction and horizontal bars mean ± s.e.m.).

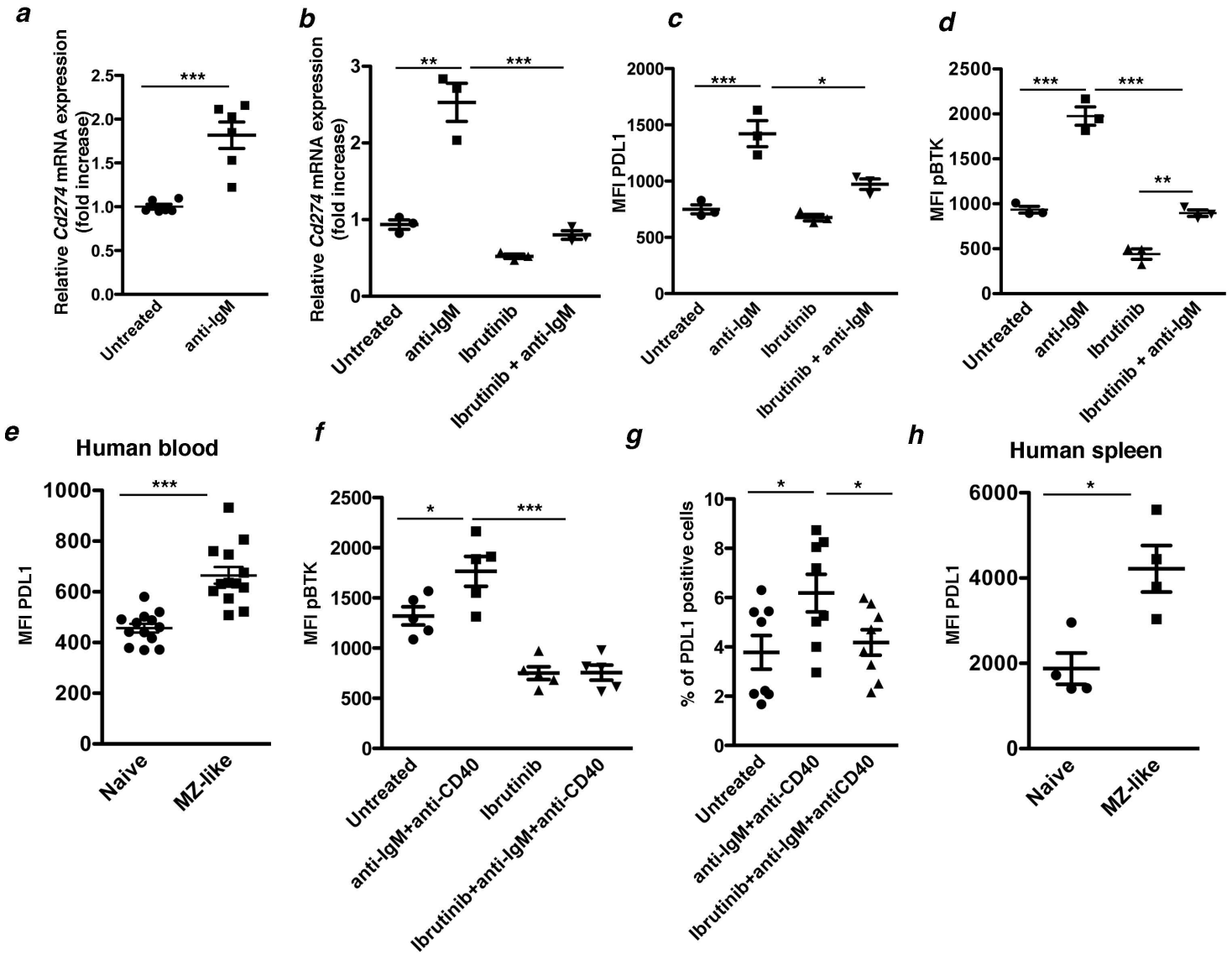

Supplementary Figure 6. Effects of BCR signaling on PDL1 expression in murine MZB cells and human MZ-like B cells. Shown are data from sorted MZB cells of WT mice, treated in vitro with anti-IgM, ibrutinib (Btk inhibitor) or both for 3 hours to assess *Cd274* mRNA (a-b), or for 6 hours to assess PDL1 protein expression by flow cytometry (c). Also shown is the phosphorylation of Btk (pBtk) analyzed by flow cytometry in the presence or absence of anti-IgM and/or ibrutinib (d). All experiments were carried in n=5 biological replicates/conditions. We also analyzed human blood (e-g) and spleen (h) B cells. (e, h) PDL1 expression using flow cytometry in naïve and MZ-like cells in blood (n=13) and spleen (n=4). pBTK (f) and percentage of PDL1 positive cells with respect to total blood B cells (g) in purified B cells treated for 18 hours with anti-IgM+anti-CD40 antibodies, ibrutinib or their combination (n=6 biological replicates/ condition). Bars represent mean ± s.e.m. * $p<0.05$; **$p<0.01$ and ***$p<0.001$.

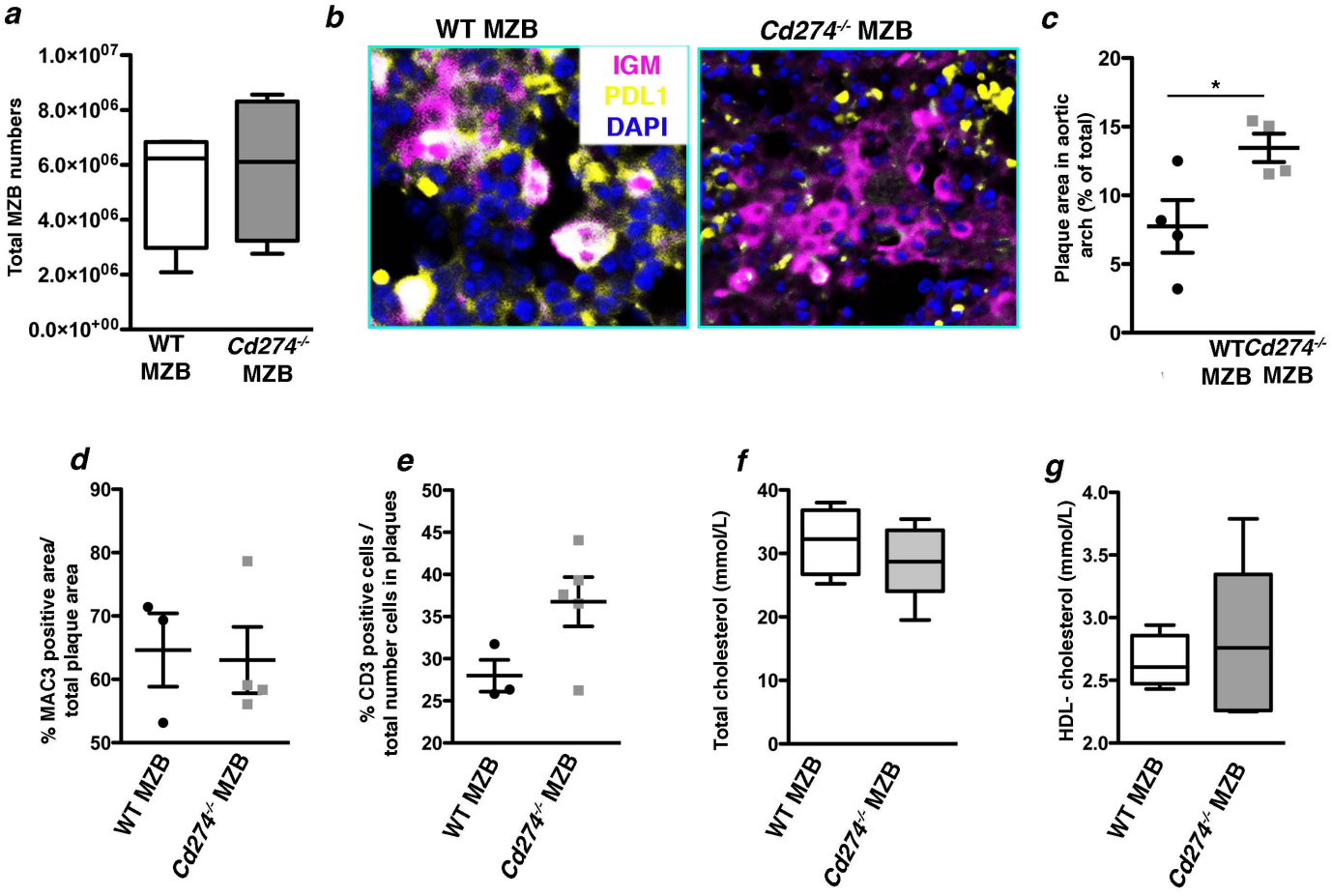

Supplementary Figure 7. Further characterization of Ldlr-/- mice with either wild type MZB cells or C274 deficient MZB cells. Shown are data from *Ldlr*$^{-/-}$ mice transplanted with a mixed BM chimera containing 80% *Cd79a*$^{Cre/+}$/*Rbpjk*$^{flox/flox}$ + 20% WT or *Cd274*$^{-/-}$ bone marrow (a-f). (a) Numbers of MZB cells in the spleens of the 2 groups of mice after BM transplantation and HCD for 8 weeks. (b) Spleen sections from WT MZB and *Cd274*$^{-/-}$ MZB groups were immunostained for PDL1 (yellow) and for IgM (magenta). White color indicates a detection of PDL1 expression on IgM^{+} MZB cells. (c) Quantification of Oil red O *en face* staining of aortic arches (with each symbol representing one animal and horizontal bars mean ± s.e.m). Quantification of Mac3 (d) and CD3 (e) positive staining in atherosclerotic plaques of aortic roots (n=4 mice/group and 3 representative sections from each mouse were analyzed). Total cholesterol (e) and HDL-C (f) levels in serum (n=5 mice/group). Bars represent mean ± s.e.m. Two-tailed unpaired Student t-test * $p<0.05$; ** $p<0.01$ and *** $p<0.001$.

Table S1. Flow Cytometry antibodies

Target	Clone	Company
B220	RA3-6B2	eBioscience
IgM	II-41	eBio
MHC-II	M5/114.15.2	Biolegend
CD23	B3/B4	eBioscience
CD21	eBio4E3	eBioscience
CD69	H1.2F3	Biolegend
CD44	1M7	Biolegend
CD4	RM4-5	Biolegend
CD3	145-2C11	Biolegend
CD62L	MEL-14	Biolegend
CD95	Jo2	BD
GL7	GL7	eBioscience
B220	RA3-6B2	eBioscience
CD19	1D3	BD
CD138	281-2	Biolegend
CD4	RM4-5	Biolegend
CXCR5	L138D7	Biolegend
ICOS	C398.4A	eBioscience
PD1	RMP1-30	Biolegend
CD274	MIH5	eBioscience
pBtk	M4G3LN	eBioscience
pSyk	Moch1 ct	eBioscience

Table S2: Primers used for qRT-PCR

	Sense	Antisense
A20	TGGTTCCAATTTTGCTCCTT	CGTTGATCAGGTGAGTCGTG
Abcg1	GGAAGATGTAGGACGGTTGG	GAGCACAGGATGGCATTCTAT
Fosb	ATGTCTCCACTCTCAATG	GTCACACTTACTTACAGAAG
Atf3	GCGAAGACTGGAGCAAAAT	TGGATGGCGAATCTCAGCTC
IL10	ATGGCCCAGAAATCAAGGA	CACAGGGGAGAAATCGATGA
Junb	GAACAGCCTTTCTATCAC	TTTCAGGAGTTTGTAGTC
Klf4	TTATTGTGTCGGAGGAAGAG	TCACCAAGCACCATCATT
Nur77	CCCACTATTTGTCTTATCC	CATCTCAACCTCTTCCTT
Ccr7	CTGAATGAACCTGCTTCT	CTTGCTAAGTGTGGAGATAA
Ebi2	TGCTGCGATTCTCTGTAAT	CTTAGGAACTTAGGAAGACCAT
Cd274	CTTCCTTCCTTCCTTCCT	GCATAGTGAGCAACCATT
Icosl	AGGAATGAGGAGTGAGAAC	ATTGAATACATCGGTGTGAAG
IL6	CCAGAGATACAAAGAAATGAT	ACTCCAGAAGACCAGAGGAAA
36B4	TCTCCAGTGGCTCCATTGA	CTCGCTGGCTCCCACCTT
Il21	AAGCAATGATGGACAGAGA	GTCAAGAAGTCAACAGTTACA
Icos	ATATGAGTTAGTTGGAAGGATT	TAGGCATACAGACAGGAA
S1pr1	TACACAGGCAAGTTGAAC	AGCAGATGAGAATGAACAC
Ascl2	TGACATCTTCCATCTTCC	GAGTCCTACAACAGTTCA
cMaf	TTCTGAGTTCTTCTGATTG	TTGATGTAGGCTTGATTG